11-1-2013

Development of a Computational Approach to Assess Hip Fracture and Repair: Considerations of Intersubject and Surgical Alignment Variability

Azhar Ali
University of Denver

Development of a Computational Approach to Assess Hip Fracture and Repair: Considerations of Intersubject and Surgical Alignment Variability

Abstract

Hip fracture remains a major public health concern due to the significant number of occurrences and mortality rates. Intertrochanteric fractures are the most common type of fracture and are typically caused by a fall. Intramedullary osteosynthesis is a common surgical practice to repair intertrochanteric fractures, but revisions are often required. The work presented in this thesis aims to improve the realism and fidelity of computational models of hip fracture, which can be an effective alternative to costly and labor-intensive clinical in-vivo and experimental in-vitro testing. Intersubject variability is inherently present in anatomy and material relations. Statistical shape and intensity models can be used to characterize anatomic and material property variability in a training set population and can be used to evaluate subject-specific fracture behavior. While prior computational models of hip fracture have evaluated bone strains to assess fracture risk, the current study advances the state of the art by utilizing a novel technique in the extended finite element method (XFEM) to assess hip fracture and develops a computational approach to evaluate fracture repair.

Natural and implanted finite element models were used to predict fracture patterns and evaluate bone-implant load share in subjects with varying geometry and bone quality. A model validation study demonstrated the capability of XFEM in generating unique subject-specific fracture patterns. Femurs generated from a previously published statistical model were fractured to capture the range of patient variability in fracture pattern and load at the onset of fracture. Overall femur size, bone thickness, and bone quality had large effects on load at the onset of fracture. Using one of the average subject models, a study was performed to investigate the effects of surgical alignment, implant material, and loading variability on hip fracture repair. Although, surgical alignment had little effect on load share in the bone-implant construct, mal-alignment caused an increase in peak implant stress and bone strain, which could result in implant failure and delayed fracture healing. Muscles were added to a fracture repair model to capture loading condition variability, which resulted in a more balanced load share between the bone and the implant, indicating the importance of musculoskeletal modeling. These studies included novel techniques for evaluating hip fracture and repair that could be used to aid the surgical community by providing guidance on how implant alignment can promote ideal bone healing conditions.

Document Type

Thesis

Degree Name

M.S.

Department

Mechanical Engineering

First Advisor

Peter J. Laz, Ph.D.

Second Advisor

Paul J. Rullkoetter, Ph.D.

Third Advisor

James N. Hagler

Development of a Computational Approach to Assess Hip Fracture and Repair: Considerations of Intersubject and Surgical Alignment Variability

_____

A Thesis

Presented to

the Faculty of the Daniel Felix Ritchie School of Engineering and Computer Science

University of Denver

_____

In Partial Fulfillment

of the Requirements for the Degree

Master of Science

_____

By

Azhar Ali

November 2013

Advisor: Peter J. Laz

Author: Azhar A. Ali
Title: Development of a Computational Approach to Assess Hip Fracture and Repair: Considerations of Intersubject and Surgical Alignment Variability
Advisor: Peter J. Laz
Degree Date: November 2013

Abstract

Hip fracture remains a major public health concern due to the significant number of occurrences and mortality rates. Intertrochanteric fractures are the most common type of fracture and are typically caused by a fall. Intramedullary osteosynthesis is a common surgical practice to repair intertrochanteric fractures, but revisions are often required. The work presented in this thesis aims to improve the realism and fidelity of computational models of hip fracture, which can be an effective alternative to costly and labor-intensive clinical in-vivo and experimental in-vitro testing. Intersubject variability is inherently present in anatomy and material relations. Statistical shape and intensity models can be used to characterize anatomic and material property variability in a training set population and can be used to evaluate subject-specific fracture behavior. While prior computational models of hip fracture have evaluated bone strains to assess fracture risk, the current study advances the state of the art by utilizing a novel technique in the extended finite element method (XFEM) to assess hip fracture and develops a computational approach to evaluate fracture repair.

Natural and implanted finite element models were used to predict fracture patterns and evaluate bone-implant load share in subjects with varying geometry and bone quality. A model validation study demonstrated the capability of XFEM in generating unique subject-specific fracture patterns. Femurs generated from a previously published

statistical model were fractured to capture the range of patient variability in fracture pattern and load at the onset of fracture. Overall femur size, bone thickness, and bone quality had large effects on load at the onset of fracture. Using one of the average subject models, a study was performed to investigate the effects of surgical alignment, implant material, and loading variability on hip fracture repair. Although, surgical alignment had little effect on load share in the bone-implant construct, mal-alignment caused an increase in peak implant stress and bone strain, which could result in implant failure and delayed fracture healing. Muscles were added to a fracture repair model to capture loading condition variability, which resulted in a more balanced load share between the bone and the implant, indicating the importance of musculoskeletal modeling. These studies included novel techniques for evaluating hip fracture and repair that could be used to aid the surgical community by providing guidance on how implant alignment can promote ideal bone healing conditions.

Acknowledgements

I would like to thank my advisors, Dr. Peter Laz and Dr. Paul Rullkoetter, for their support and insight into the field of computational biomechanics. Their passion in research inspired me to become involved in biomechanics and expand my abilities. Their guidance over the past four years as an undergraduate and graduate student helped define a direction for my career. I would also like to thank Dr. Clare Fitzpatrick, Dr. Chadd Clary, Dr. Milind Rao, and Dr. Kevin Shelburne for providing me many hours of support and technical assistance. They were instrumental in helping me learn the foundations of finite element modeling and providing the tools and skills I need to be successful in my research. I also need to thank the graduate students who supported my work: Chandreshwar Rao, James Deacy, Tariq Abo-Alhol, Lowell Smoger, and John Ivester.

I would like to acknowledge Luca Cristofolini at the University of Bologna in Bologna, Italy, and Enrico Schileo and Fulvia Taddei from the Rizzoli Institute of Orthopaedics in Bologna, Italy, and Sebastian Eberle and Peter Augat from the Institute of Biomechanics in Murnau, Germany for providing experimental data in support of this study.

Lastly, I would like to acknowledge the Osteosynthesis Trauma Care Foundation and the University of Denver for supporting this study.

Table of Contents

List of Figures

List of Tables

Chapter 1. Introduction

Based on the significant number of occurrences and the resulting postsurgical outcomes, hip fractures are a major public health concern. High mortality rates following hip fracture and large numbers of surgical revisions show the need for continued hip fracture and repair research. Previous works have characterized fracture behavior using clinical testing, experimental testing, and computational modeling. Clinical studies have identified geometric and bone quality measures associated with fracture risk. Experimental testing has been performed to assess fracture load and characterize overall bone strength. Computational modeling studies have used maximum and minimum principal strains to identify highly strained regions, which can be related to fracture risk. While clinical in-vivo and experimental in-vitro testing can prove to be labor-intensive and costly, computational modeling of natural and implanted hip fracture can help avoid surgical revisions and identify shape and bone quality characteristics of subjects most susceptible to fracture. It is known that there is intersubject variability in anatomy and bone quality (Laz et al., 2007). Previous work has addressed interpatient geometric and material variability using statistical shape and intensity models from principal component analyses. Mechanical testing and finite element modeling in literature have applied femoral fall and stance loading conditions, and have considered the effects of implant selection and alignment. Based on previously developed, techniques, the current project improves the realism and fidelity of computational models of hip fracture and repair.

Fracture patterns are influenced by patient factors, including geometry and bone quality. Computational models of hip fracture were developed to predict fracture patterns in femurs under common injury loading conditions for a series of subjects with varying geometry and bone quality representative of the population. To capture the range of geometry in the population, an existing, published statistical shape and intensity model was used to create a series of 'virtual' subjects that represent the most common modes of variation. Patient variability in fracture patterns was assessed by sampling up to 5 principal component modes within +/- 2 standard deviations. While prior computational studies have used maximum and minimum principal strains to identify regions of high fracture risk, most studies have not considered the direction of this min/max strain in the element, which would indicate how a crack would propagate through the bone. In the current study, fracture predictions utilized the recently-developed extended finite element method (XFEM) in the Abaqus finite element software (Dassault Systems, Providence, RI) to determine the location of crack initiation and the path of crack propagation. XFEM applies energy-based fracture criteria to determine crack growth through a structure, and is not required to travel along specific element boundaries. This novel approach was used to predict fracture patterns in subjects with varying geometry and bone quality.

Computational models were developed to simulate the repair of hip fractures with intramedullary osteosynthesis devices for the population of subjects fractured using XFEM, including the impact of patient and surgical alignment variability. The integrity of the model was maintained and a more realistic evaluation of surgical repair was

performed by using the same representation of geometry and bone quality as in the fracture study, and including the specimen-specific fracture surface from XFEM. Previous computational models of fracture repair have evaluated peak implant stresses and bone strains, but the current study also considered the impact of bone geometry and alignment variability. Computational models also characterized the load distribution in the construct, considering how much load is carried by the implant, the fracture, and the surrounding bone. The surgical repair model can be used to investigate the healing process and identify optimal loading conditions for fracture healing.

Accordingly, the objectives of the current study were to predict fracture patterns in femurs under common injury loading conditions for a series of subjects with varying geometry and bone quality representative of the population, to validate predicted fractures with experimental testing, and to model the repair of hip fractures with intramedullary osteosynthesis devices for the same population of subjects, including the impact of variability in surgical alignment, implant material, and loading conditions. Hip fracture and repair modeling can be used to identify subject-specific features associated with fracture risk and recommend implant alignment parameters that balance the structural integrity of the implant and ideal bone healing conditions.

1.1 Organization

Chapter 2 highlights the motivation for the work and previous studies of hip fracture and repair. Clinical, experimental, and computational modeling studies of hip

fracture are discussed in order to expand and improve the current study. Also, the fracture methodology used in the following chapters is discussed in detail.

Chapter 3 provides a specimen-specific analysis of hip fracture and repair. It compares the fracture methodology to experimental data in order to validate the model. Specimens are evaluated elastically using localized strain gages and loaded until failure. Model stiffness, localized strain, and fracture pattern are compared to the experiment. Specimen models are, then, fractured under common injury loading conditions and repaired to evaluate implant stresses, bone strains and load transfer.

Chapter 4 investigates the effects of patient, alignment, implant material, and loading condition variability on hip fracture and repair. Subjects are generated from an existing statistical shape and intensity model and fractured under fall loading conditions. Fracture patterns and load at the onset of fracture are evaluated for each subject. Each subject is repaired to evaluate the effects of patient variability in hip fracture repair. An average repair model is investigated with varying surgical alignment, implant material, and loading conditions to determine sources of variability in fracture repair.

Chapter 5 provides concluding remarks and recommendations on the current study. It highlights the capability of the computational hip fracture and repair platform, and also recommends future work to advance the model.

Chapter 2. Background Information

2.1 Hip fracture: Motivation and Background

Approximately 1.6 million hip fractures occurred worldwide in the year 2000 (Johnell and Kanis, 2006). Mortality rates at 1 year following hip fracture were approximately 22% for men and 14% for women in 2005 (Brauer, Coca-Peraillon, et al., 2009). According to the American Association of Orthopaedic Surgeons, there were approximately 281,000 hospitilizations due to hip fractures, and 90% of hip fractures result from a fall (Cummings and Melton, 2002; Hall et al., 2010). Intramedullary osteosynthesis is a common surgical intervention to treat frequently occurring intertrochanteric fractures. Revisions are required in up to 12.6% of the cases due to implant failure or delayed fracture healing (Raunest et al., 2001). Due to the significant number of hip fractures and uncertainty in post-surgical outcomes, hip fractures are a major public health concern.

The clinical relevance hip fracture and repair modeling and analysis is multifold. Implant alignment parameters that most significantly influence the bone strain and implant stress distributions can be identified. Also, studying hip fracture can be used to recommend implant selection and alignment based on specific patient features in order to realize more optimal load transfer conditions. Additionally, the model findings can aid the surgical community by providing guidance on how implant alignment, and

rehabilitation protocol influence the distribution of load in the construct in order to avoid surgical revisions. Lastly, the natural modeling can aid in identifying at-risk populations by identifying the shape and bone quality characteristics of subjects most susceptible to hip fracture.

2.2 Clinical In-vivo and In-vitro Fracture Testing

Clinical in-vivo studies have identified geometric and bone quality measures associated with fracture risk. Geometric measures include neck-shaft angle, intertrochanteric width, and femoral head diameter. Bone quality measures include osteoporosis, bone mineral density, bone turnover, and biochemical markers. Clinical studies have used CT, MRI, DEXA, quantitative ultrasound (QUS), and biochemical markers to measure geometric and bone quality factors associated with fracture risk. Clinical research typically utilizes a large dataset of patients over the course of several years to identify risk factors in the population; for example, the data from Osteoporotic Fractures in Men (MrOS) has been used in several studies to classify at-risk populations (Bauer et al., 2009, 2007). Clinical in-vivo studies can identify at-risk populations by recognizing shape and bone quality characteristics associated with fracture.

Intraoperative measures can be used to judge the quality of the proximal femur prior to surgical intervention. Fritscher et al., (2009) assessed local bone quality of the proximal femur based on model-based CT and X-ray images of femur specimen. A statistical model was used to isolate features of the images to assess bone mineral density. Algorithms were tested and applied to 28 femur specimen. The study successfully measured bone mineral density. The modeling technique provided an in-vivo, non-

invasive analysis of bone quality to predict high risk regions of fracture and isolate at-risk populations. Krug et al., (2005) has also shown that high resolution MRI scans can be used to assess the trabecular microstructure of the proximal femur. With some proper tuning and calibration, MRI has the potential to map bone quality and identify weak regions of the femur. Advances in imaging technology prove to be a powerful tool for evaluating bone quality. Bone turnover has also been used to measure accelerated bone loss. Although bone turnover is typically measured using bone biopsy specimens, biochemical measurements using bone turnover markers (BTM) has been shown to link processes of bone resorption and formation (Bauer et al., 2009). BTM can be used to predict bone quality and identify fracture risk populations. In addition to CT, MRI, and BTM, Bauer et al., (2007) showed that quantitative ultrasound (QUS) can also be used to predict hip fracture with the same level of accuracy as hip bone mineral density.

Geometric measures of shape and size can also correlate with fracture risk. Prior studies have used measurements of geometric features of the proximal femur to predict hip fractures. Based on the Study of Osteoporotic Fractures (SOF), (Kaptoge et al., 2008) used hip structural analysis software to derive geometric variables associated with fracture risk. Statistical analysis was performed on 635 femurs from the fracture database to predict the incidence of hip fracture. The relative size of the neck, intertrochanter, and shaft regions were significant. Large neck-shaft angles, subperiosteal diameter, and lateral distance were correlated to hip fracture. In addition, a cohort study using MrOS was designed to examine the effects of bone mass, bone geometry, lifestyle, neuromuscular measures, and fall propensity on hip fracture risk (Orwoll et al., 2005). A

series of geometric and lifestyle variables associated with fracture risk were identified using questionnaires. Geometric variables are significant in fracture prediction and they can be used pre-operatively to identify at-risk populations.

Experimental cadaveric testing has been performed to assess fracture load and characterize overall bone strength. Mechanical testing of bones help identify realistic femur stiffness and material properties. Experimental testing provides quantitative validation based on mechanical properties (strain and displacement) (Cristofolini et al., 2010; Keyak et al., 2001). Computational modeling has complemented experimental testing by investigating a number of loading conditions, and perturbing material property and interface parameters.

2.3 Computational Modeling Fracture Studies

Many finite element studies of hip fracture and repair have used bone strain distributions and peak implant stresses to identify at-risk populations and evaluate fracture repair (Bryan et al., 2009; Cristofolini et al., 2010; Eberle, Gerber, et al., 2010). Prior modeling efforts have used minimum and maximum principal strains to identify regions of high fracture risk (Bryan et al., 2009). An improved modeling technique for crack initiation and crack propagation including geometry and material variation is a valuable tool for understanding the dynamics of hip fracture. The current study initiates and propagates cracks utilizing the extended finite element method (XFEM) in Abaqus (Simulia, Providence, RI) (Liu et al., 2010). The purpose of this project is to improve the realism and fidelity in computational models of hip fracture and to develop an approach

to consider the effects of implant alignment and patient factors on hip fracture repair with an osteosynthesis implant.

The hip fracture and repair research project utilizes previously developed work considering geometric and material variability in the femur. Subject variability is often overlooked in orthopaedic computational studies due to challenges in generating large numbers of bone models. A statistical shape and intensity model (SSIM) of the whole femur has been developed to incorporate both geometric and material property variation in order to address intersubject variation (Bryan et al., 2010). A statistical model was constructed using principal component analysis (PCA) applied to 46 individual computed tomography scans. The statistical model tested the ability to generate realistic, unique, FE femur models and it was used to create 1000 femurs to study femoral neck fracture risk. The development of a PCA statistical model for femoral fracture risk can be used for future FE models to not only predict stress and strain distribution, but also crack initiation and propagation. Taking into account development of intersubject variability can make future FE fracture models more robust.

In order to create an accurate femur model, a method for mapping bone material properties is necessary. Using CT and MRI scans, gray-scale values can be converted to density. Several relationships have been identified between elastic modulus and density for trabecular and cortical bone using CT scans (Keyak and Falkinstein, 2003; Les et al., 1994; Morgan et al., 2003; Rho et al., 1995). In Morgan et, al, (2003), elastic moduli and apparent densities were measured from 146 human trabecular bones ranging from vertebrae, proximal tibia, femoral greater trochanter, and femoral neck. Resultant power

law regressions have been identified from measured values and depend on anatomic site. Each bone material relationship study has identified different power law regressions relating modulus to density. They have also identified variability in yield strains and stresses for bone. Since finite element models of bones are generally used to address clinical problems by evaluating their response to mechanical loading, subject-specific FE models have to be highly reliable and be able to predict mechanical parameters with sufficient accuracy. However, there is a considerable amount of uncertainty in material property relations and each subject model has its own specific density-elastic relationship (Eberle et al., 2012). Computational models must be validated in order to predict fracture/mechanical behavior of a series of subjects. Even though material relations are subject-specific, a cohort-based material relation, such as Morgan et al. (2003), can be used to define bone properties and predict fracture for a population. In order to simulate bone fracture, basic experimental data on bone fracture toughness properties is needed. There are experimental data in support of a power law relationship for the fracture toughness as a function of the density of the tissue (Cook and Zioupos, 2009). Power law regressions with proven anatomic dependency allow appropriate material mapping to the bone to increase the complexity of a bone fracture analysis.

2.4 Fracture Repair Using Intramedullary Osteosynthesis

The choice of the appropriate implant continues to be critical for fixation of unstable hip fractures. Unstable hip fractures are cracks susceptible to continued propagation through the bone. Surgical treatments implementing osteosynthesis implants

aim to stabilize bone fracture by transferring load share to the implant. Common clinical practice supports the use of an intramedullary osteosynthesis device to stabilize and repair intertrochanteric fractures. The success of surgical treatment depends on bone quality, fracture pattern, fracture reduction, implant design, and implant alignment (Kaufer, 1980). Prior studies of fracture repair have attempted to identify the optimal implant design, alignment and fracture reduction conditions in order to support the surgical community. Eberle et al. (2010) developed a numerical model to investigate the mechanical performance of hip fracture osteosynthesis. Understanding the relationship between interfragmentary movement and fracture stability is crucial when treating hip fracture cases. Mechanical testing and a finite element analysis were developed for a cephalomedullary nail within a synthetic femur and simulated a pertrochanteric, lateral neck, and a subtrochanteric fracture (Eberle et al., 2009). Intramedullary implants (tested using FE models and strain gages) can stabilize unstable hip fractures with almost the same amount of stiffness as seen in stable fractures. Eberle et al. (2009) supported clinical techniques for repairing fractured femurs using intramedullary implants and compared the stiffness, and stress distributions in three fracture types. The load share in implants in comparison to three fractures types can be used to create properly aligned and bounded implant models. An implanted femur FE model can be generated and validated using the implant-bearing fracture data.

Computational models of hip fracture repair have been developed to predict the bone strain distribution and implant stresses following surgical intervention. Prior studies have validated models using in-vitro synthetic femurs (sawbones) or a small number of

subjects/cadavers (Eberle, Gerber, et al., 2010; Eberle et al., 2009). In order to identify causes of post-surgical femoral neck fracture, the influence of various metaphyseal stem configurations (diameter, percentage length in contact with bone, and bonded versus debonded) and cement mantle thickness on the load transfer within the resurfaced femoral head are important to consider. Taylor et al. (2006) showed that resurfacing the femoral head resulted in significant strain shielding in the superior femoral head and elevated strain in the superior femoral neck. Although the increase in strain in the femoral neck was significant, the mean strains were not significantly above the yield strain, so it was unlikely that the bone would fracture. Increasing the stem diameter and increasing the percentage stem length in contact with bone both increased the degree of strain shielding. Bonding the metaphyseal stem produced the most dramatic strain shielding and cement mantle thickness had a negligible effect. Taylor et al. (2006) considered crucial factors in an implanted, resurfaced femoral head that could cause increased stress leading to bone fracture. When creating future hip fracture repair models, the ideal implant stem configurations and alignments can be used to simulate healthy, stable surgical repairs.

Because there are a large number of surgical revisions from implant failure, it is important to address the question of how the stability of a proximal hip fracture determines the fatigue and failure mechanism of an intramedullary nail. Mechanical experiments and FE simulations were performed on two loading conditions comparing two different mechanical supports of the fracture using an artificial bone sleeve (Eberle, Bauer, et al., 2010). An intramedullary nail fails at a load 28% lower with an unstable

fracture support than with a stable support. Mechanical support of a fracture is important to the fatigue failure of an implant. (Fatigue occurs at the aperture of the lag screw with the highest von Mises stress.) Eberle et al. (2010) provided detailed insight towards a properly, stable-supported implant to avoid implant fracture and fatigue.

Although previous investigations of hip fracture and repair have considered geometric and material variability, and appropriate boundary and loading conditions, and implant selection and some alignment variability, there are areas of research that can be improved. Previous PCA-developed statistical shape models may be limited because they used a relatively small set of CT femurs to predict the population (Bryan et al., 2009). The data set does not incorporate factors such as osteoporosis and tumors since the data was taken from a general, healthy population. In order to account for a wider range of geometric and material variability, a PCA-developed statistical shape model could be developed for different genders, ages, ethnicities and pathologies. The boundary and loading conditions applied in mechanical testing arbitrarily represented femur fall and stance conditions (Keyak et al., 2001). Previous loading conditions may not represent realistic fall conditions. Including muscle attachment sites and forces can improve the realism of computational models and provide a more educated loading condition. Hexahedral and tetrahedral elements were used in the models and the mesh density was very coarse, which could cause significant error. The stress-strain data at the bone surface is unreliable because the models had an irregular geometry. Most modeling and mechanical testing of implant repair used synthetic femurs, which approximate the material properties and complexities of bone tissue (Eberle, Bauer, et al., 2010). It also

represents a healthy population only and ignores pathological variations in geometry and material properties. Computational finite element models in the past have used stress-strain distributions to approximate fracture locations and have excluded realistic subject-specific fracture patterns.

2.5 Extended Finite Element Method

Bone fracture analysis using the Extended Finite Element Method (XFEM) in Abaqus can be used to predict fracture behavior of bone tissue to suggest surgical treatment options and take preventative measures. XFEM is a meshless technique to model the location of crack initiation and the path of crack propagation without a priori knowledge of crack path.

Numerical results from XFEM have compared well to experiments (Song et al., 2007) and for both 2-D and 3-D complex geometries including material non-linearity (Gracie et al., 2008; Huynh and Belytschko, 2009). XFEM method is compared to other fracture finite element techniques such as the element deletion method and interelement crack method (Song et al., 2007). XFEM compares well to analytical solutions and proves to be a promising technique for studying brittle fractures. The technique has also been used to study fracture in composite materials. Several numerical examples of 2-D and 3-D structures with complex material properties (eg. multi-fiber composite cell) illustrate the versatility of the technique (Huynh and Belytschko, 2009). Liu et al. (2010) have first applied the technique to predict bone fracture in a proximal femur under impact. The technology is capable of simulating crack patterns and predicting bone

fracture based on various loading conditions. XFEM technology is an advanced computational modeling technique that can be used to simulate fracture with crack initiation and propagation to generate fracture patterns on femurs.

2.5.1 Methods

For the following chapters of the study, a standard methodology was used for the development of XFEM models. Fracture property assignment and loading conditions were consistent for most of the fracture studies.

For subject-specific models, bone geometry was reconstructed from the CT scans in ScanIP. Scans had a pixel size of approximately 0.5 mm and a slice thickness of 0.6 mm. For statistical shape and intensity models, bone geometry was generated as variations from a previously described population set. A mesh was created to represent each femur model consisting of approximately C3D4 (Abaqus linear TET element type) tetrahedral elements with average element edge lengths of 1 mm in the proximal section of the femur. Material properties were assigned to each element based on the grayscale values from the CT scans. Density and Young's modulus were mapped to the femur using the Bonemat software (Istituto Ortopedico Rizzoli, Bologna, Italy). Density was calculated from a linear relationship between Hounsfield units (HU) and density (Peng et al., 2006; Schileo, Dall'ara, et al., 2008) and Young's modulus was determined from a density-based power law regression for the femoral neck (Morgan et al., 2003).

$$\rho_{app}\left(\frac{g}{cm^3}\right) = 0.00134375 * HU \text{ (Peng et al., 2006)}$$

$$E\ (MPa) = 6850\rho_{app}^{1.49} \text{ (Morgan et al., 2003)}$$

The femur models were subjected to two loading conditions: stance and fall. The stance condition was a ramped load applied to the femoral head at 0 or 8 degrees adduction in the frontal plane and simulated a resultant hip joint load during stance. The femur was encastred along the shaft axis. The fall loading condition applied a load to the femoral head at 20 degrees anteversion and 30 degrees rotation along the long axis of the femur. The fall loading condition simulated an oblique fall backwards and to the side (Keyak, 2000) with the applied load ramped until fracture.

Fracture was modeled using XFEM, which applies strain and energy-based criteria to determine the location of crack initiation and the subsequent path of crack propagation. A static analysis was performed to predict the bone strain distribution and identify the region at risk of fracture. An enriched region, where fracture is permitted to occur in the XFEM analysis, was defined based on the strain results and excluded elements adjacent to the boundary and applied loading conditions. Crack initiation occurred in elements when principal strains exceeded 0.61% (Morgan and Keaveny, 2001). Crack propagation was predicted by critical strain-energy release rates, G_{IC}, G_{IIC}, and G_{IIIC} for mode I, II and III fracture types, which are a function of density (Cook and Zioupos, 2009). Since the fracture path is a combination of all the modes of fracture, a constant G_{IC} to G_{IIC} and G_{IIIC} ratio was assumed based on (Zimmermann et al., 2009).

$$K_{IC}\left(MPa\sqrt{m}\right) = 0.7413\rho_{app}^{1.49} \quad \text{(Cook and Zioupos, 2009)}$$

$$G_{IC} = \frac{K_{IC}^2}{E*(1-\nu^2)}$$

2.5.2 ASTM Tensile and Torsion Test Example

As a proof of concept, the XFEM technique was applied to an ASTM standard geometry (E8) with uniform material property distribution. The diameter of the middle section of the specimen was chosen to be 30 mm to match an average femoral shaft diameter. The remaining dimensions of the specimen were scaled to match ASTM standards (E8) for a tensile and torsion test. The geometry consisted of a C3D8 hexahedral mesh with an average element length of 1 mm. The model was given a uniform material property definition; it was linear, elastic with a Young's modulus of 1000MPa and a Poisson's ratio of 0.3. Fracture properties were defined as described above in the previous section. Crack initiation was the same as the bone yield strain criterion, 0. 61%. Crack propagation was defined by strain energy release rates, which are a function of fracture toughness and density.

The ASTM model was subjected to two loading conditions: tension and torsion. Initially, the model was subject to an axial load of 100kN for the tensile load configuration and a 500Nmm torque for the torsion load configuration. To compare fracture convergence in displacement control versus force control, the model was subjected to displacements corresponding to its force-loaded counterparts. The model was pulled axially by 2.5mm and twisted by 0.5mm. The model was fixed in all degrees of freedom at one end and load was applied to the other end for each loading condition.

Fracture patterns in the ASTM geometry matched analytical solutions. When loaded under tension, fracture propagated perpendicular to the load. When loaded under torsion, fracture propagated at a 45 degree angle.

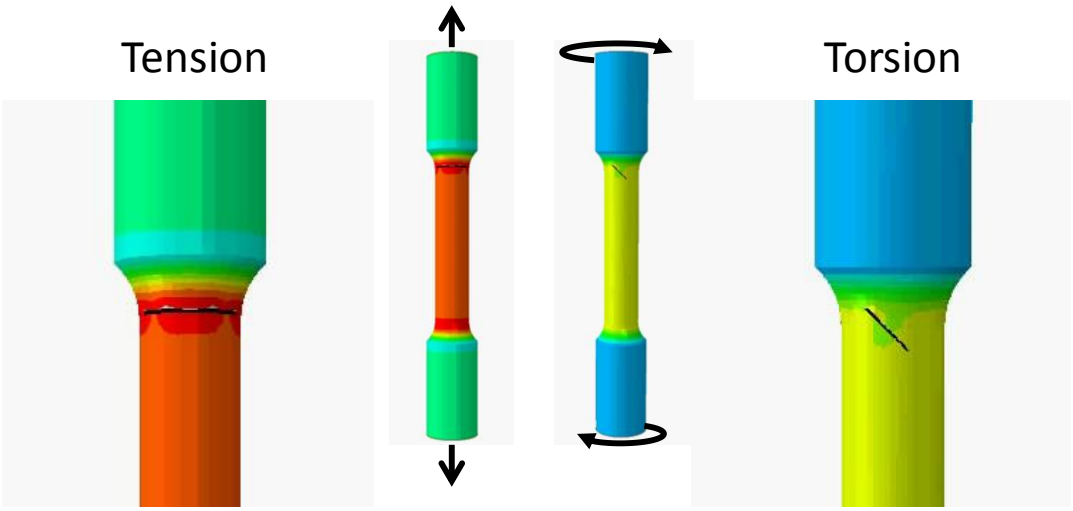

Figure 2.1: Fracture pattern with strain distribution on ASTM geometry during tension (left) and torsion (right)

The ASTM tension and torsion test validated the fracture methodology using the XFEM technique. XFEM was able to predict accurate fracture patterns of a standard geometry and they matched analytical solutions. Fracture patterns shown in Figure 2.1 did not propagate through the entire specimen. Displacement control did not significantly improve fracture convergence. Results indicate that mesh refinement in the enriched region may be required for further convergence and crack propagation.

Chapter 3. Specimen-Specific Modeling of Hip Fracture and Evaluation of Repair

3.1 Introduction

Hip fracture remains a significant public health concern as a result of the high incidence and consequence. Approximately 1.6 million hip fractures occurred worldwide in the year 2000 (Johnell et al., 2006) with approximately 281,000 hospitalizations due to hip fracture in the United States in 2007 (Hall et al., 2010). Mortality rates at 1 year following hip fracture were approximately 22% for men and 14% for women in 2005 (Brauer et al., 2009). In the United States, approximately 90% of these fractures are the result of a fall (Cummings et al., 2002), with many occurring in the intertrochanteric region of the femur. This type of fracture is typically repaired with an intramedullary osteosynthesis device to provide stability to the reduced fracture. While implant design and the overall procedure is generally successful, surgical revisions are required in up to 12.6% of the cases due to implant failure or delayed fracture healing (Raunest et al., 2001).

Many studies have investigated factors that influence hip fracture, specifically patient anatomy, bone quality and loading. In vivo studies have identified clinical measures associated with osteoporosis and fracture risk (Fritscher et al., 2009; Kaptoge et al., 2008; Krug et al., 2005). Experimental cadaveric testing has been performed to assess fracture load and characterize bone strength on whole bones (Cristofolini et al.,

2010; Keyak, 2000) and on small samples (Morgan and Keaveny, 2001; Morgan et al., 2003). For both types of testing, specimen specific computational models have been developed to parallel the experiments. Specimen-specific models are typically created from computed tomography (CT) or microCT scans which enable a detailed representation of the anatomy of the bone and its material properties (Keyak et al., 2003; Schileo et al., 2008A, Ural et al., 2013A). The validation of models by showing good agreement with in vitro data (Schileo et al., 2007, Trabelsi et al., 2011; Eberle et al., 2013; Dall'Ara et al., 2013) provides confidence in the techniques that will enable their application more broadly to patients in the clinic. Combined experimental and modeling studies have investigated the femur under stance and fall loading conditions in both the intact natural (Cristofolini et al., 2010; Keyak, 2000) and fracture repaired condition (Eberle et al., 2010). Both the experimental and modeling data contain a significant amount of variability, likely attributed to intersubject variability in bone properties (Taddei et al., 2006A; Laz et al., 2007; Wille et al., 2012; Eberle et al., 2013).

Computational studies have identified regions of high minimum and maximum principal strain (Bryan et al., 2009; Taddei et al., 2006B), which are related to the fracture location and risk. Recently, studies have utilized a variety of FE-based techniques to advance the modeling of bone fracture including: cohesive zone elements to model a crack at microstructural and macro levels (Ural et al., 2013A,B), homogenized continuum-level voxel models (Dall'Ara et al., 2013), continuum damage mechanics methods using bone remodeling and element deletion (Hambli, 2013A, Hambli et al., 2012, 2013B), and the extended finite element method (XFEM) which models crack

initiation and propagation independent of the mesh (Belytschko et al., 1999). By predicting the damage accumulation and fracture pattern, these fracture-based approaches implemented within finite element analysis show promise in providing more mechanistic predictions of bone fracture.

As a complement to the standard finite element method, XFEM introduces a Heaviside function that allows discontinuities in an element by adding enriching degrees of freedom to the element formulation (Belytschko et al., 1999). A specialized displacement function is evaluated for enriched elements by considering a max principal stress/strain damage initiation criterion to model fracture onset and an energy-based damage evolution criterion to model fracture propagation, which includes the redistribution of strain ahead of the crack tip as the crack grows. The XFEM approach has been implemented in the Abaqus finite element software (Dassault Systems, Providence, RI). In benchmarking, numerical results from XFEM have compared well to experiments (Song et al., 2007) and for complex geometries including material non-linearity (Gracie et al., 2008; Huynh et al., 2009). In orthopaedic biomechanics, XFEM has been applied to investigate the fracture of ceramic hip liners (Elkins et al., 2013) and demonstrated in a proximal femur under impact loading (Liu et al., 2010). The approach is similar to using cohesive zone elements with the notable difference that the XFEM approach does not require a priori knowledge of the crack path.

Computational models evaluating fracture repair have characterized the implant stresses and bone strain distribution using idealized fracture planes (Eberle et al., 2010). However, fracture patterns, influenced by anatomy and bone quality, vary greatly

between subjects. By creating subject-specific fractured models, the XFEM modeling approach can be utilized as a platform to evaluate the performance of implant designs and the effects of component alignment considering intersubject variability. Mechanical stimuli across the fracture are known to be important in the healing process, although the ideal conditions are not well understood (Doblaré et al., 2004). The computational platform can predict bone strains near the fracture and load sharing between the implant and bone fracture surface in the repaired construct, which influence the local conditions for healing. Given its image-based, computational nature, the approach can be employed to investigate patient cohorts, including those in at-risk populations, and utilized in design-phase evaluations of implants, including assessments of their robustness to patient and surgical variability sources.

Accordingly, the objectives of this study were to predict femoral fracture in specimen-specific models using the XFEM approach, to perform one-to-one comparisons of predicted and in vitro fracture patterns, and to develop a framework to assess the mechanics and load transfer in the fractured femur when it is repaired with an osteosynthesis implant. Initially, specimen-specific femur models of in vitro experiments were developed under a stance loading condition to validate the approach. Then, to consider fracture repair, a sideways fall loading condition was applied to the specimen-specific femur models to induce an intertrochanteric fracture, which was repaired with a contemporary intramedullary osteosynthesis device. Simulating post-surgical conditions, implant stresses, bone strains and load sharing between the implant and fracture were evaluated under stance loading.

3.2 Methods

3.2.1 Experimental Setup

In vitro testing was performed on five cadaveric femurs (3 male, 2 female, mean age of 75.2 (range 71-82), mean height of 173 cm (range 166-178 cm) and mean weight of 69.6 kg (range 43-91 kg)) per an established testing protocol (Cristofolini et al., 2010). Prior to mechanical testing, specimens were CT-scanned (HiSpeed, GE Co., USA) immersed in water with peak voltage and tube current levels typical of clinical examinations, together with a phantom containing known densities (European Spine Phantom (Kalendar, 1992)). In the experimental setup, strain gage rosettes were placed on the anterior, posterior, medial, and lateral femoral head, neck, trochanteric and metaphyseal regions of each femur. The femurs were oriented and loaded to simulate stance (Figure 3.1). The femur was aligned by rotating the long axis of the femur to 8° adduction in the frontal plane. The distal femur was potted in bone cement fixing the femoral shaft in all degrees of freedom (Table 3.2). Initially, an elastic loading condition, consisting of an applied inferior-superior load equivalent to 75% of body weight, was applied to evaluate bone stiffness. The structural stiffness was computed as the slope of the load-cell force vs. machine-actuator deflection curve (linear regression between 10% and 90% of the full load). Strain gage rosette measurements were used to measure the

maximum and minimum principal strains in local regions of the femur (Figure 3.2). Subsequently, loading was ramped until failure of the specimen while high speed photography at ~18,000 frames/sec captured the fracture progression (Cristofolini et al., 2007; Juszczyk et al., 2011). Applied displacement rates were nominally 2 mm/s and 20 mm/s (Table 3.2) resulting in strain rates on the order of 5,000 and 50,000 microstrain/second in the most stressed regions and fractures occurring in 2 and 0.2 seconds, respectively.

3.2.2 Fracture Model Development

Finite element (FE) models were developed for each of the cadaveric femurs. Bone geometry was reconstructed from the CT scans using ScanIP (Simpleware, Exeter, UK). Scans had a pixel size of approximately 0.5 mm and a slice thickness of 0.6 mm. A mesh was created to represent each femur consisting of approximately 594,492 C3D4 tetrahedral elements with average element edge lengths of 1 mm in the proximal region and 5 mm in the distal region (726,532 total degrees of freedom). This mesh size was established following evaluations of convergence in models with meshes ranging from 0.5 mm to 3 mm. Material properties were assigned to each element based on the grayscale values from the CT scans (Tables 3.1 and 3.2). Density and Young's modulus were mapped to the femur using the Bonemat software (Taddei et al., 2004). Density was calculated from a linear relationship between Hounsfield units (HU) and density (Schileo

et al., 2008B), and Young's modulus was determined from a density-based power law regression for the femoral neck (Morgan et al., 2003).

Fracture was modeled using XFEM in Abaqus, which applies strain and energy-based criteria to determine the location of crack initiation and the subsequent path of crack propagation. A static analysis was performed initially to assess the bone strain distribution and identify the region at risk of fracture. An enriched region, where fracture was permitted to occur in the XFEM analysis, was defined based on the strain results and excluded elements adjacent to the boundary and applied loading conditions. Given the tensile-dominated loading of the enriched fracture region, crack initiation was defined to occur in elements when principal strains exceeded 0.61%, derived for tensile strains in the femoral neck and greater trochanter (Morgan et al., 2001). Crack propagation was governed by critical strain-energy release rates, G_{IC}, G_{IIC}, and G_{IIIC} for mode I, II and III fracture types. Energy release rate, G_{IC}, for trabecular bone was a function of density (Cook et al., 2009), and since fracture path could be a combination of multiple modes of fracture, a constant ratio of G_{IIC} and G_{IIIC} to G_{IC} was assumed based on Zimmermann et al. (2009).

3.2.3 Model Validation

To validate the modeling approach, a one-to-one comparison between model and experiment was performed for each specimen. The models were oriented and loaded to reproduce the experiment (Table 3.2). Overall stiffness of the femur was calculated by

dividing the applied load by the overall displacement of the femoral head. Specific nodes on the surface of the femur model were identified to match the position of the strain gage rosettes in the experiments. Maximum and minimum principal strains were averaged over the surface elements adjacent to each "strain gage" node during the elastic loading. After comparing stiffness and localized strains, the FE models were fractured under the stance loading condition. The load at crack onset and the crack path were compared to the experimental data and high speed and post-test photographs.

3.2.4 Fracture Repair

In this portion of the study, the fracture modeling approach was employed to create a series of specimens with intertrochanteric fractures and then an intramedullary osteosynthesis device was implanted virtually to evaluate the mechanics of the repaired construct. A fracture analysis using XFEM was performed for each specimen-specific model under the sideways fall loading condition. Simulating an oblique fall backwards and to the side (Keyak, 2000), the fall loading condition applied a ramped load to the femoral head at 20° anteversion and 30° rotation along the long axis of the femur (Figure 3.1). Cracked elements from the XFEM analysis were identified and defined the fracture surface. It should be noted that the fracture in the model did not always propagate through the entire bone due to convergence issues with a crack growing parallel to an element edge length. In these cases, the developed crack plane was extended through the remaining intact bone. An orthopaedic surgeon identified the appropriate size and

alignment of the intramedullary osteosynthesis implants to repair the fractured femur. The position of the lag screw was established with an appropriate tip-apex-distance, which is intended to optimize fixation clinically. The femurs were remeshed with C3D4 tetrahedral elements to include the implants and the fracture interface, and the density and modulus properties were reassigned. Implant geometries were also represented with tetrahedral elements. Average element edge lengths were 1 mm resulting in approximately 553,149 and 116,922 elements for bone and implants, respectively (856,934 total degrees of freedom). Contact was defined between the mating faces of the fracture surface with a frictional coefficient of 0.46 (Eberle et al., 2010). Bone-to-implant and implant-to-implant contact interactions were represented with frictional coefficients of 0.3 and 0.23, respectively (Eberle et al., 2010). Simulating post-surgical conditions, the repaired models were subjected to loads of 75% of body weight under the stance loading condition. Load sharing was evaluated by considering the normal and shear reaction forces along the fracture surface and carried by the bone and implant. The reaction forces were calculated by multiplying element contact stresses by their respective cross-sectional areas, thus also incorporating forces due to moments. In addition, the stresses in the implant and strain distribution in the bone near the fracture surface were computed.

3.3 Results

Using material relationships from the literature, the models reproduced the material behavior from the experiments for all 5 specimens. Comparing results for the elastic applied load in the stance configuration, predicted maximum and minimum principal strains for the various strain gage locations agreed well with the experimental values (Figure 3.2). Model predictions were correlated (R^2) to the experiment at 0.92 with a slope of the regression curve of 0.96 for 68 strain gages across the 5 specimens; average differences between model and experimental strains were 32% for all specimens. Model stiffness underpredicted the experimental measurement for all specimens, but was within 25% (Table 3.2). Balancing strain results and convergence of the XFEM analysis which favors large elements, mesh convergence was established by differences in peak and average strains in the enriched region of less than 4.8% between analyses performed with the 1 mm and 0.5 mm meshes.

Fracture patterns matched closely between the XFEM analyses and in vitro tests with all tests and analyses resulting in neck fractures under stance loading. The side-by-side comparisons of model and experiment show good agreement in the fracture location and path when compared to the high speed and post-test photographs (Figures 3.3 and 3.4). Influenced by crack initiation at a single element, loads at the onset of fracture from the model were significantly smaller (approximately 50%) than the experimental fracture loads (Table 3.3).

When subjected to the simulated sideways fall loading condition, the XFEM analyses predicted intertrochanteric fracture patterns that were consistent with fall fractures observed clinically (Figure 3.5). The repaired construct consisting of the fractured bone and intramedullary osteosynthesis implants was evaluated under stance loading to assess the altered mechanics and load transfer (Figure 3.6). Contact pressures were distributed distally on the fracture surface, which is expected given the applied stance loading. The normal and shear reaction forces for the bone and implant were averaged over the fracture surface (Table 3.4) and indicated that the implant carried a majority of the load. The load distribution ranged from 59% to 89% carried by the implant and 41% to 11% carried by the bone, with an average load sharing of 73% implant to 27% bone for the 5 specimens. The load sharing was influenced by how the plane of fracture intersected the bone and implant as shown by differences in the fracture plane area and fracture angle (Table 3.4, Figure 3.6). Implant stresses were greatest at the interface between the lag screw and the nail (Figure 3.6). Notably, peak von Mises stresses in the implants and peak bone strains in the near fracture region varied between models (Table 3.4).

Computational times for the XFEM fracture analyses were 5-10X those of traditional static analyses. The XFEM analyses required only minor modifications to the input files associated with a static analysis, essentially assigning the fracture-related material properties and defining the enriched region.

3.4 Discussion

This study presented a computational approach to predict specimen-specific femoral fracture patterns, which can be used to investigate fracture in at-risk clinical populations and support the design of osteosynthesis implants. The predicted fracture patterns are unique to each specimen as they are dependent on anatomy and bone quality. The fracture patterns developed using XFEM closely matched experimental testing and those observed clinically. Recently, advances in fracture modeling have enabled finite-element based evaluations of the crack initiation and propagation processes, including predictions of fracture patterns (Hambli et al., 2013B, Dall'Ara et al., 2013). The XFEM approach used in this study modeled the onset of cracking using the maximum principal strain yield criterion and determined the direction and amount of crack propagation using an energy-based damage evolution criterion. As a crack grows, the analysis redistributes loading as the crack surfaces are not able to transfer load in tension and the crack tip behaves as a stress singularity. A strength of the XFEM approach using enriched elements is that the fracture path is determined by the analysis and does not need to be specified in the mesh as with cohesive zone element approaches (Ural et al., 2013B). In contrast to continuum damage-based approaches using microCT or microstructure, by using generalized fracture properties assigned from CT, this work represents a macro approach with potential for more broad applications in the clinic and in implant design. Fracture analyses with XFEM can be performed with only minor modifications to the

model input files for a traditional strain-based evaluation, yet provide a more mechanistic evaluation of the fracture process.

The predicted overall mechanical behavior and fracture patterns agreed with in vitro testing for the specimens evaluated; however, some differences in stiffness, strain and fracture load were observed between model and experiment, at a level consistent with other published studies (Trabelsi et al., 2011; Eberle et al., 2013). Material properties were mapped to the bone model from CT scan data using a phantom to calibrate density and published material relations. While this is an accepted approach, many studies have noted the large variability present in these relationships (Eberle et al., 2012; Laz et al., 2007; Helgason et al., 2008; Wille et al., 2012) and their influence on the mechanical behavior, though comparative studies have been performed (Schileo et al., 2007). In a blinded validation study, Trabelsi et al. (2011) reported correlations (R^2) of 0.95 with a slope of 1.04 and errors of 22% in strain and correlations of 0.62 and errors of 45% in stiffness between model and experiment. Investigating three commonly used material relations, Eberle et al. (2013) showed the smallest errors of 11% in strain gage and 23% in stiffness when comparing model and experimental results using the relation from Morgan et al. (2003). Using the same material relation, our results with correlations of 0.92 for strain and differences of 25% in stiffness are consistent with the accuracy of these other studies, and representative of how the approach could be applied to a new subject when detailed experimental data are not available.

Additionally, the predicted load at the onset of fracture was considerably smaller than in the experiment, which is likely due to the as-mentioned property differences and

sensitivity to the thin cortical bone layer on the surface of the femur. Discretization during the segmentation process can lead to artificially soft elements on the bone surface. The fracture analyses are more sensitive to the local surface material properties than traditional strain analyses, as fracture begins at a single weakest element rather than the element being one of many that experiences high strains. To show sensitivity, when the yield strain criterion was increased from 0.61% to 1% (Bryan et al., 2009), the load at the onset of fracture increased by approximately 36%. While care should be taken in interpreting the model results in terms of failure load, the good comparisons with stiffness, strain and fracture path corroborate the model for further use in comparative studies of bone fracture and bone-implant interaction.

The XFEM analysis experienced some issues with convergence as cracks did not always propagate all the way through the bone; this convergence issue was caused by the computational challenge of solving for a crack running parallel to an element boundary. The majority of prior XFEM analyses have been performed on engineered components with uniform geometry and material that allows a crack to propagate cleanly through large elements (Areias et al., 2005; Elkins et al., 2013; Hughes et al., 2010). In this study, a relatively fine tetrahedral mesh (~1 mm element edge length) was required to accommodate the natural bone geometry and distribution of material properties; however, this mesh also increased the likelihood of the crack aligning with an element edge. Cracks propagated further by modifying XFEM control parameters, e.g. increasing the number of increments and iterations, and decreasing the minimum step size. Alternatively, remeshing has been suggested as a way to improve model convergence for

crack propagation (Gracie et al., 2008), but will still be problematic given the complex geometry and material property distribution. While specifying a crack path in the mesh, similar to with cohesive zone elements, would improve model convergence, the XFEM approach considers subject-specific factors of anatomy and bone quality by determining the path of crack propagation within the analysis

Computational models of fracture provide an ideal platform to evaluate the devices and practices used to repair fracture as they capture intersubject variability in anatomy, bone quality and fracture pattern. The approach can also quantitatively assess the impact of implant selection and alignment on the performance of the fracture repair. Other studies have evaluated load transfer of implant-repaired models with idealized, virtual fracture planes (Eberle et al., 2009). The current study is unique in that it utilized the XFEM approach to generate specimen-specific fracture planes representative of anatomic and material property variation. The repair analyses predicted stresses in the implant, strains in the bone near fracture, and the load transfer across the fracture. The need for subject-specific evaluations was shown by the differences in the bone-implant load sharing between the models, which were influenced by the orientation of the fracture and the relative cross-sectional areas of the bone and implant across the fracture plane. For example, Specimen 2 had a small implant cross-sectional area (14% of total fracture area) and resulted in a more even load distribution (41% carried by implant and 59% by bone), while Specimen 5 had a larger implant cross-sectional area (27% of total fracture area) and resulted in the implant carrying more of the load (89% carried by implant and 11% by bone). Fracture pattern also influenced the compression and shear components

of the loading across the fracture. The repeatability of the fracture repair methods was assessed by recreating the orientation of the fracture plane from the fall analysis. Variations in percent load transfer were less than 3%. While further validation is needed, the platform can provide insight into load sharing across the fracture, which is important as mechanical stimuli are known to influence the bone healing process (Doblaré et al., 2004).

The main limitation of the current study is the sensitivity to the local surface material properties. As discussed, fracture load at onset was most sensitive to the absolute density value of a single element. The current study assumed homogenous linear isotropic material properties and did not consider the known anisotropic behavior of bone. Lastly, the study presented results for 5 specimens and would be strengthened with larger numbers of specimens and additionally, direct comparisons to in vitro testing under the sideways fall loading condition.

In closing, this study has demonstrated the ability of the XFEM approach to predict specimen-specific fracture patterns. Fracture models enable investigations of patient cohorts and can characterize how fracture patterns are influenced by anatomy and bone quality in at-risk populations. As there continue to be cases of implant failure and malunion (Raunest et al., 2001), the approach shown can be applied to improve the design of implants and the performance of fracture repairs, considering the structural integrity of the implant and the local mechanical conditions for bone healing.

T**able 3.1:** Relationships used to assign material properties in the model from CT image data.

Relationship	Source
ρ-QCT (g/cm^3) = 0.00079114*HU – 0.00382144 ρ-ash (g/cm^3) = 0.877*ρ-QCT + 0.0789 ρ-app (g/cm^3) = ρ-ash/0.6	Schileo et al., 2008B
E (MPa) = 6850*ρ-app$^{1.49}$	Morgan et al., 2003
ε critical = 0.061	Morgan et al., 2001
K ($Nm^{-1.5}$) = 0.7413E6 $\rho^{1.49}$ Converted to G (J/m^2)= $K^2/E*(1-\mu^2)$	Cook et al., 2009
$G_{IIC}/G_{IC} = G_{IIIC}/G_{IC}$ = 0.33	Zimmermann et al., 2009

Table 3.2: Summary of material properties for each specimen-specific model, experimental loading conditions and comparison of stiffness. Note: Differences in experimental stiffness between specimens 1-2 and 3-5 were primarily due to the location at which the specimens were fixed distally.

	Young's Modulus (MPa)			Distal Fixation (% length from	Loading	Applied Elastic Load	Stiffness (N/mm)	
Specimen	Min	Max	Avg	distal end)	Rate (mm/s)	75% BW (N)	Experiment	Model
1	417.1	23763.2	6174.5	2/3	20	470	1448	1128
2	401.8	24035.4	5342.6	2/3	20	464	1348	1048
3	484.4	23892.0	8008.8	1/3	2	672	630	514
4	524.5	23441.0	7585.2	1/3	2	576	818	622
5	449.0	24471.0	7051.5	1/3	2	540	534	317

Table 3.3: Load at the onset of fracture: experiment and model-predicted under stance loading and model-predicted under fall loading.

	Fracture Load for Stance Condition		Fracture Load for Sideways Fall Condition
Specimen	Experiment (N)	Model (N)	Model (N)
1	4555	3270	2327
2	5803	2388	2067
3	8041	3927	3030
4	6443	3018	3297
5	6344	1964	2897

Table 3.4: Predicted load sharing and cross-sectional area for the bone and implant across the fracture interface, bone strains and implant stresses for each repaired femur.

Specimen	Load Share N (%)		Frac. Angle	Cross Sectional Area mm^2 (%)		Bone Strain Min Principal (mm/m)		Peak von Mises Implant Stress
	Implant	Bone	(°)	Implant	Bone	Mean	St.Dev.	(MPa)
1	3102 (83)	625 (17)	53.7	495 (23)	1673 (77)	-511	1150	114.3
2	1118 (59)	774 (41)	46.9	302 (14)	1912 (86)	-234	288	47.7
3	2362 (73)	863 (27)	55.3	387 (13)	2685 (87)	-169	264	62.6
4	841 (61)	545 (39)	52.8	611 (26)	1780 (74)	-181	265	87.8
5	3431 (89)	432 (11)	55.5	749 (27)	2039 (73)	-281	297	98.6
Avg.	1971 (73)	648 (27)	52.8	509 (20)	2018 (80)	-275	453	82.2

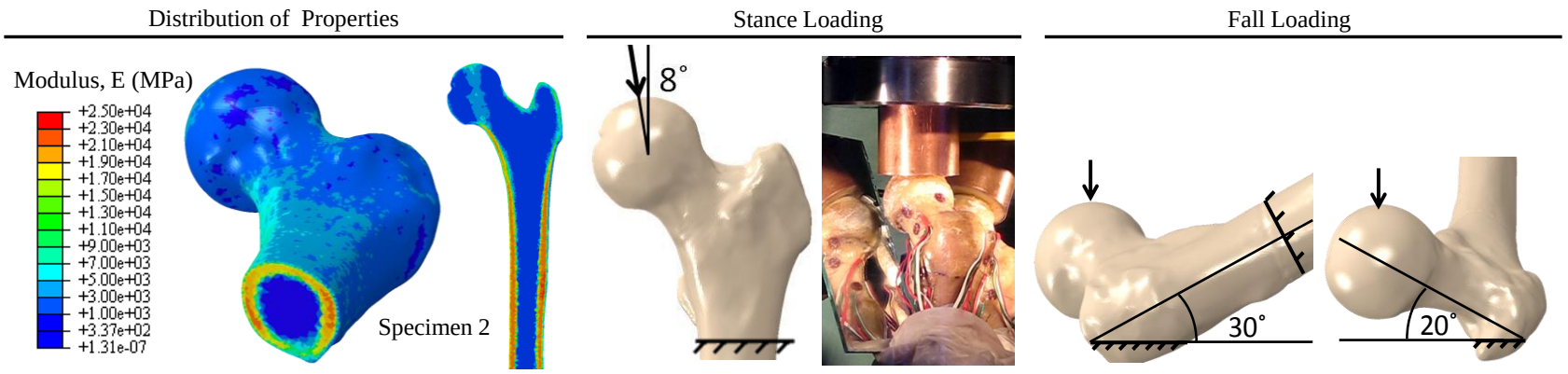

Figure 3.1: Bone geometry showing mapped material properties with applied loading conditions simulating stance (Cristofolini et al., 2010) and fall loading conditions (Keyak, 2000).

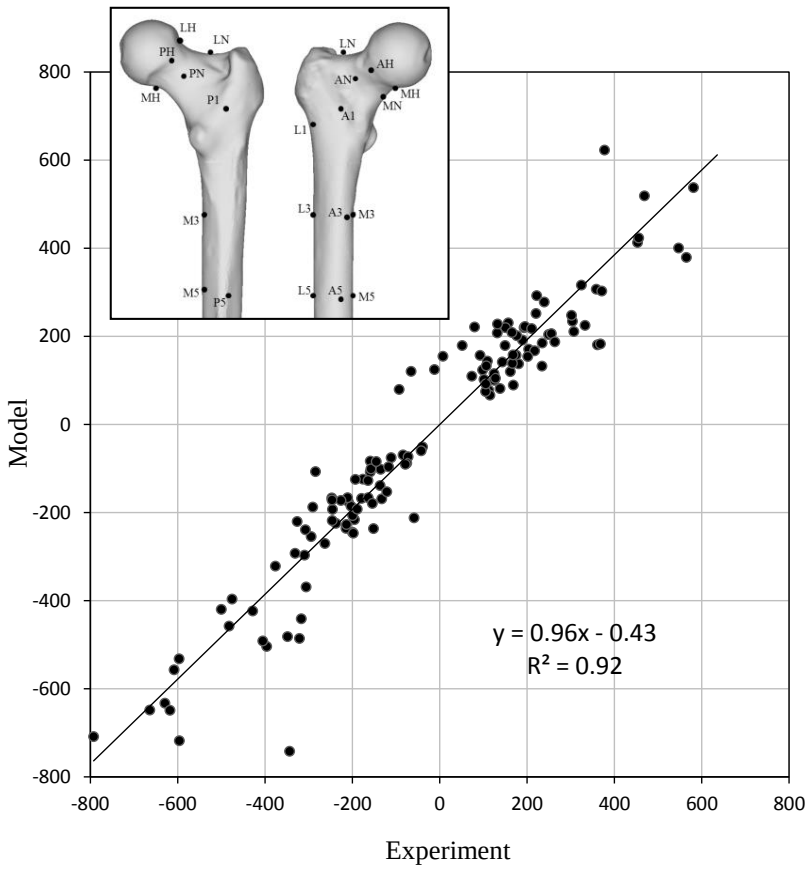

Figure 3.2: Comparison of localized strain measurements (max and min principal) between the experiment and model for all five specimens under elastic stance loading. Inset: locations of strain gages. AH, LH, PH, MH – anterior, lateral, posterior and medial head; AN, LN, PN, MN – anterior, lateral, posterior and medial neck; A1, L1, P1 – anterior, lateral and posterior proximal diaphys; A3, L3, P3, M3, A5, L5, P5, M5 – anterior, lateral, posterior and medial distal diaphysis.

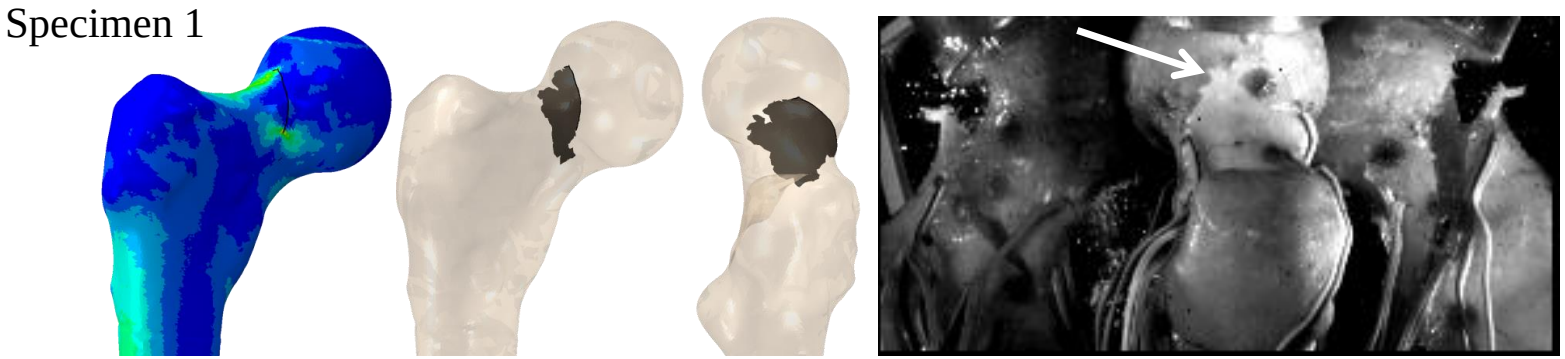

Figure 3.3: Comparison of model and experiment for each specimen under stance loading: strain distribution and model fracture (left) and experiment with mirrors showing side views (right).

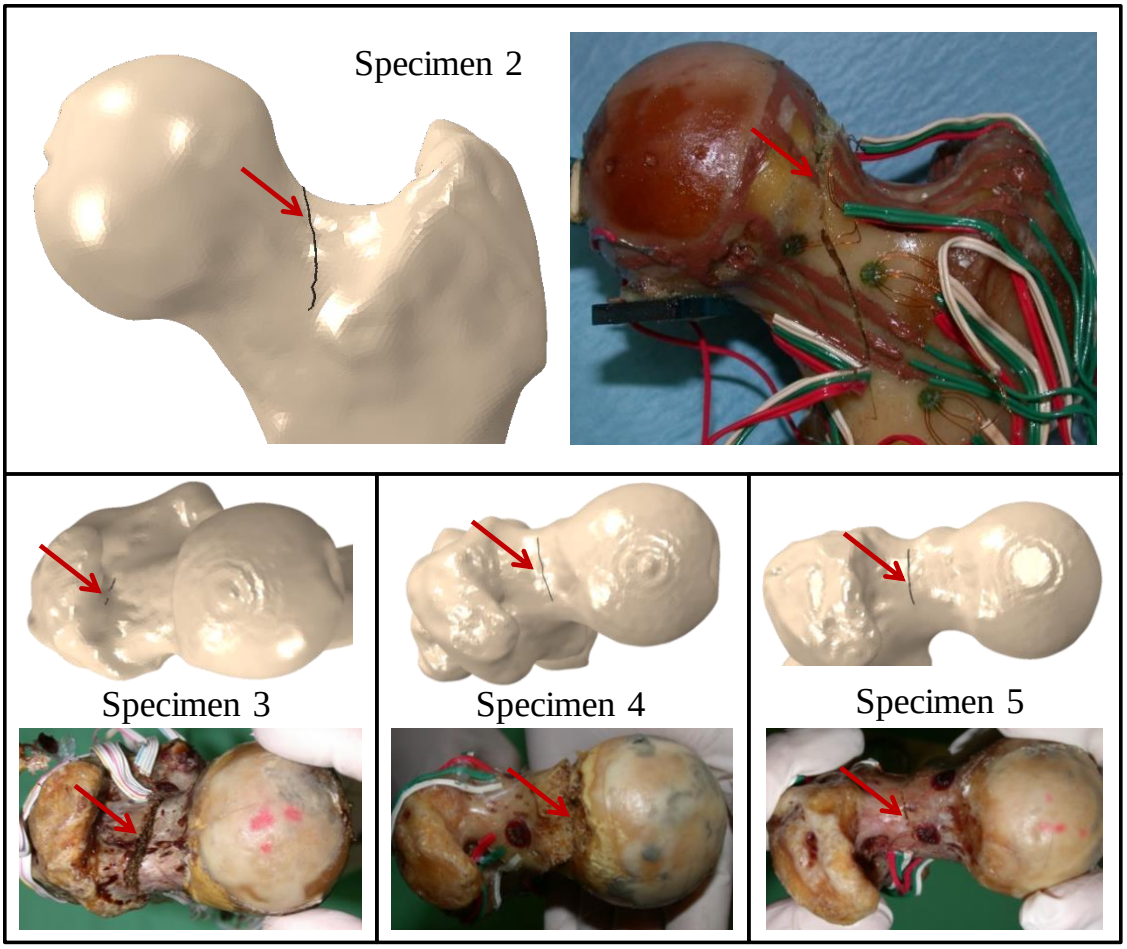

Figure 3.4: Fracture pattern comparison between model and experiment for specimens 2-5 under stance loading.

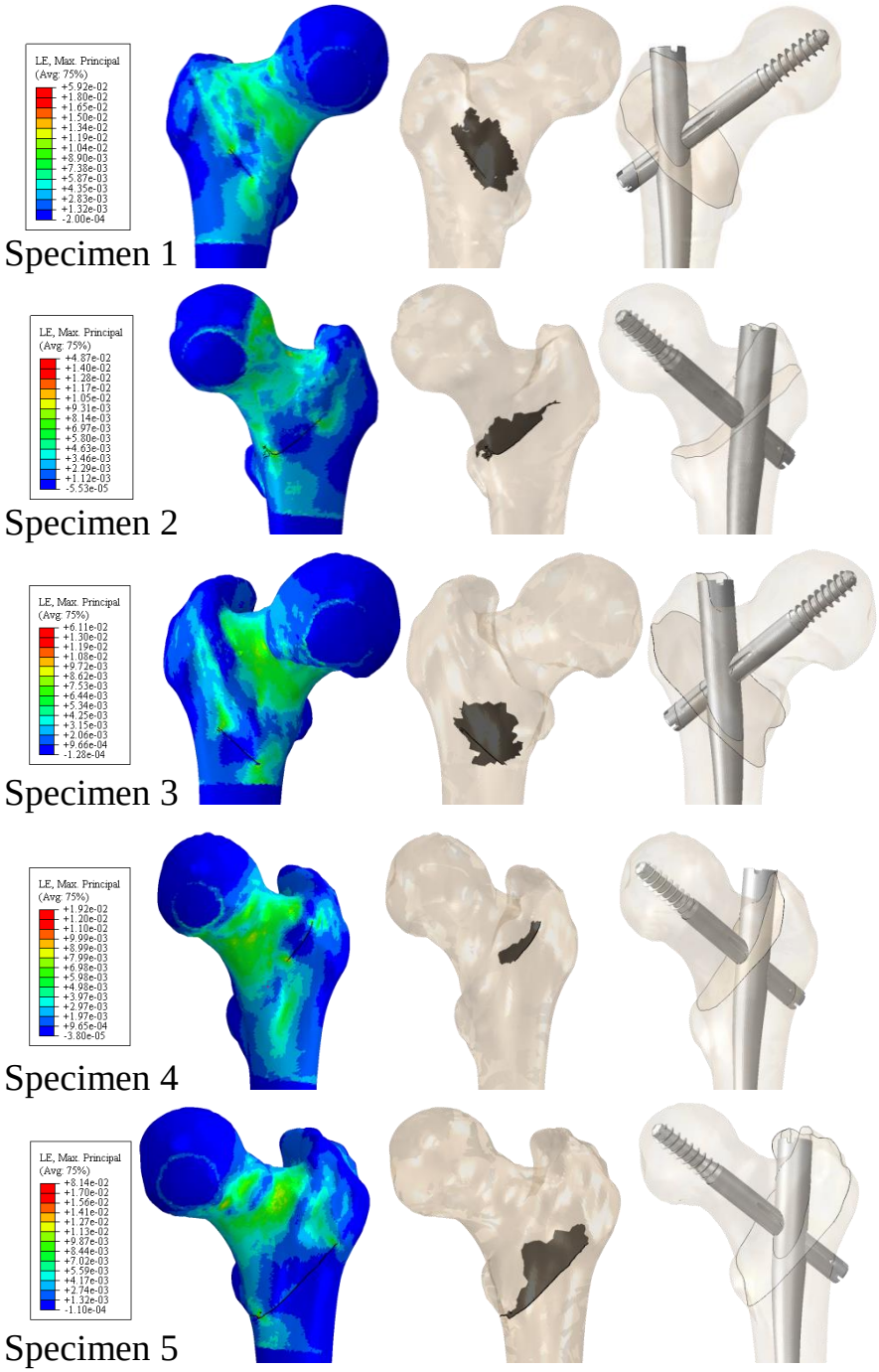

Figure 3.5: Fracture and repair process: fracture under sideways fall loading showing strain distribution (left) and fracture path (middle); repair of fractured specimen with an intramedullary implant (right).

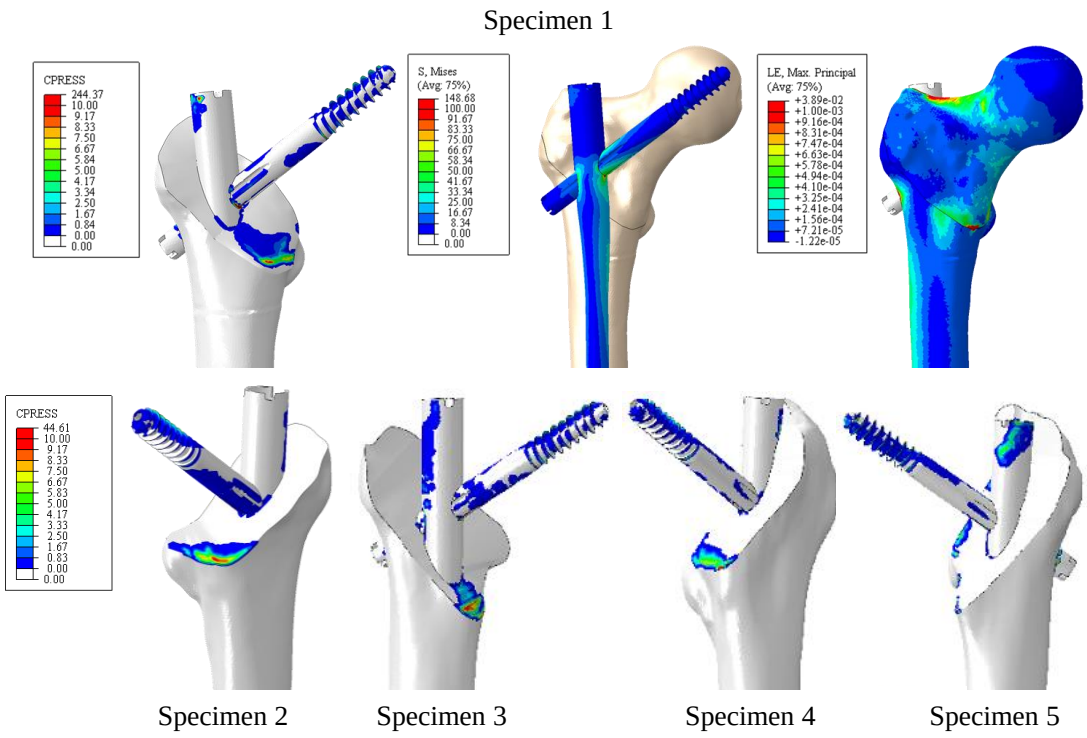

Figure 3.6: Model-predicted contact pressure distribution at the interface, stress distribution in the implant and strain distribution in the bone for Specimen 1. Contact pressure distributions for Specimens 2-5.

Chapter 4. Effect of Intersubject, Alignment, and Loading Variability on Hip Fracture Repair

4.1 Introduction

Patient-specific factors, including anatomy and bone quality, are known to influence the likelihood of hip fracture and the fracture orientation. Recently, statistical models have characterized intersubject variability in femoral shape and intensity and been applied to evaluate bone strains in a population of subjects for a simulated fall condition (Bryan et al., 2010, 2009). While prior modeling efforts have used minimum and maximum principal strains to identify regions of high fracture risk, the current study initiated and propagated cracks utilizing the extended finite element method (XFEM) in Abaqus (Simulia, Providence, RI). XFEM fracture analyses of 2-D and 3-D uniform geometry including non-linear material properties have compared well to experimental data (Gracie et al., 2008; Huynh and Belytschko, 2009; Song et al., 2007).

The ability to consider populations of 'virtual' subjects has grown significantly with the development of statistical shape modeling. Statistical shape and intensity models (SSIM) characterize the common modes of variation within a training set of subject models derived from CT scans. A statistical shape and intensity model of the femur based on a training set of 46 subjects was developed by Bryan et al. (2010) and was utilized in the current study. By utilizing this existing, published statistical model,

the SSIM can be used to create patient-specific models representing the range of possible subjects in the population.

Computational models have also been developed of hip fracture repairs to predict the bone strain distribution and implant stresses following surgical intervention. These studies have emphasized model validation using in-vitro synthetic femurs (sawbones) and cadaveric specimens, and have generally considered a neutral well-aligned implant alignment (Eberle et al., 2009; Eberle, Gerber, et al., 2010). By using unique subject-specific fracture patterns from XFEM, this study seeks to improve the realism and impact of these models by including the effects of intersubject and surgical variability. Computational models of hip fracture repair can be used to evaluate the performance of implant design and the effects of implant alignment.

Accordingly, the objective of this study was to predict hip fracture behavior in a series of statistical model-generated subjects with varying geometry and bone quality, to evaluate fracture repair by considering the load transfer across the fracture surface, and to determine the effects of surgical alignment, implant and loading condition variability on fracture repair. The purpose was to evaluate loads at the onset of fracture and the path of crack propagation for each femur model considering the most significant modes of variation, and, then, to repair the femurs with an intramedullary osteosynthesis implant to evaluate load sharing at the bone-implant construct.

4.2 Methods

4.2.1 Description of Statistical Shape and Intensity Model

A series of models representing the most common modes of variation were created from the statistical shape and intensity model. The statistical model of the whole femur was trained by 46 subject-specific femur models extracted from CT scans (mean age=70)(Bryan et al., 2010). Capturing 45% of the variability, Mode 1 represented scaling with an increase in anteversion angle. Mode 2 (8%) characterized thickening of the bone with reductions in highest modulus (cortical) bone, increases in medullary cavity volume and decreases in neck-shaft angle. Mode 3 mainly consisted of material property variability (Figure 4.1). There was an increase in maximum cortical modulus (15215 to 16357 MPa) and average bone modulus (7657 to 8629 MPa). There were also subtle changes in geometry with an increase in femoral head diameter, condylar size, lateral inclination of the femoral shaft, anteversion, and a reduction of bowing in the shaft in the sagittal plane. Mode 4 was a combination of competing mechanisms. There was an increase in neck-shaft angle, neck diameter, and intertrochanteric width, but also a decrease in maximum cortical bone modulus and a reduction of bowing in the frontal plane. Mode 5 was a combination of geometric shape variability influencing femoral head diameter, femoral shaft width, and intertrochanteric width. Also, there was an increase in average bone modulus.

4.2.2 Patient Variability in Hip Fracture

Geometry and bone properties were derived from the previously published statistical shape and intensity model. The boundary conditions reproduced an experiment simulating an oblique fall backwards and to the side (Keyak, 2000). The fall loading condition applied a load to the femoral head at 20 degrees anteversion and 30 degrees rotation of the long axis of the femur (Figure 4.2). The femur was fixed along the shaft axis.

Initially, an elastic body weight load (666 N) was applied to each femur model to identify peak bone strain regions. An enriched region was selected based on the peak strains for each subject. A load of 5 times body weight (3330N) was applied to the femoral head over 1 sec. Fracture was modeled with XFEM in Abaqus, which applies stress and energy-based criteria to determine the location of crack initiation and the path of crack propagation. Similar to modulus and strength, the energy release rate, G_{IC}, was a function of density with a constant G_{IC}/G_{IIC} ratio (Cook and Zioupos, 2009; Zimmermann et al., 2009). Details of the fracture setup are described in Chapter 2 under 2.5.1 Methods. Load at the onset of fracture was evaluated for each femur model.

In order to obtain the range of experimental fracture load data, a best and worst case scenario were generated by superposing the previous modes of variation. The best case scenario model consisted of the best combination of modes: minus 2 standard

deviations from mode 1, 2, and 5; and plus 2 standard deviations from mode 3. The worst case subject was a combination of plus 2 standard deviations from mode 1, 2, and 5, and minus 2 standard deviations from mode 3. It is important to note that the best and worst subjects capture a very small fraction of the variability and they are not representative of the population. The purpose of creating these subjects is only to bound the range of model data.

4.2.3 Patient Variability in Hip Fracture Repair

For the most significant PCA modes (1 and 2), femurs were fractured with an enriched region focused on the trochanteric region to generate clinically relevant fractures for surgical repair. An intramedullary osteosynthesis implant was sized and aligned by an orthopaedic surgeon for each subject model. Load sharing across the fracture, implant and surrounding bone was evaluated. Cracked elements from the XFEM analysis were superposed onto the repaired construct to generate a unique model-specific fracture plane. Femurs were remeshed with C3D4 elements to include the fracture plane and the implant construct. Modulus, density and fracture properties were reassigned to the repaired bone models using a custom Matlab script. The script used an iterative closest point algorithm to assign material properties from the original statistical model mesh to the new repaired mesh. The Matlab script was capable of reading alphanumeric text in order to isolate node numbers, element numbers, and material properties (density and modulus). The script required files containing the original mesh

nodes, elements, and material properties, and the new mesh nodes and elements. Contact was assigned at each of the three interfaces: bone-bone (0.46), bone-implant (0.3), implant-implant (0.23) (Eberle, Bauer, et al., 2010). Repaired models were loaded under a stance loading condition. Load (1866N) was applied at the femoral head in 0 degrees adduction in the frontal plane and the femoral shaft was fixed in all degrees of freedom (Eberle, Gerber, et al., 2010).

4.2.4 Surgical Alignment Variabilty

From the statistical shape and intensity model, the repaired mean subject was used for evaluating perturbations in implant alignment. For each implant perturbation, the femur model was remeshed with C3D4 tetrahedral elements and an average element edge length of 1mm in the proximal section of the femur. Material properties were reassigned to the femur using a custom Matlab script. In addition to modulus and density, fracture parameters such as fracture toughness, K, and critical strain energy release rates, G, were assigned to the femur using the methodology described in Chapter 2. The repaired model consisted of commercially-available intramedullary implants, and a fracture plane derived from an XFEM analysis simulating a fall backwards and to the side. The repaired model was evaluated under a stance loading condition (Keyak, 2000).

Implant perturbations on the neutral alignment were performed as recommended by an orthopaedic surgeon. The range of the alignment variability was captured in two key degrees of freedom: a superior-inferior shift of the implant construct, and an internal-

external rotation of the implant construct (Figure 4.3). Implants were shifted and rotated plus and minus 5 mm in the superior and inferior direction, and plus and minus 5 degrees version and anteversion while maintaining a consistent tip to apex distance (TAD). The translations and rotations represented the extremes of surgical alignment variability. For each implant perturbation, the location and orientation of the fracture plane remained consistent. Frictional contact remained consistent with the previously described fracture repair models. Models were loaded under the stance condition. Load share between the bone and implant was evaluated across the fracture interface for each implant perturbation. Peak implant stresses and bone strains were also calculated.

4.2.5 Implant Variability

Material properties of the implant were altered to investigate the effects of implant variability on load share, peak implant stresses, and peak bone strains. Implant material properties were changed from a titanium alloy (Ti-6Al-4V; E = 113.6GPa, v = 0.34) to PEEK (polyether ether ketone; E = 3.6GPa, v = 0.4). The mean subject from the statistical shape and intensity model was used to evaluate fracture repair for each implant material model. Frictional contact between each of the three interfaces (bone-bone; bone-implant; implant-implant) was consistent with the previously described fracture repair models. Femur models were subjected to the stance loading condition. It should be noted that implant geometry was not altered, only the implant material properties were changed.

4.2.6 Loading Condition Variability

The mean repaired subject in the SSIM was used to evaluate differences in loading conditions on fracture repair. Muscles are known to influence joint loading and contact. Including muscle representation in the finite element model could alter load share between the bone and implant, and affect peak implant stress and bone strain. A previously described load profile simulating in-vivo conditions and considering muscle and joint loads was explored (Heller et al., 2005). The subject femur was aligned to (Heller et al., 2005) using probed points on the surface of the hip muscle model. The loading condition simulated peak muscle forces during a gait cycle and included pooled muscles representing hip contact, intersegmental resultant force, abductor muscles, tensor fascia latae (proximal and distal), and the vastus lateralis. The provided lines of action were used for each muscle group and the femur was fixed distally along the shaft-axis. Frictional contact, bone properties, and fracture plane remained consistent with the previous fracture repair setup.

4.3 Results

4.3.1 Effects of Intersubject Variability in Hip Fracture

Fracture patterns and load at the onset of fracture were evaluated in models representing the range of shape and density of the population. Fractures occurred on the boundary of the neck and intertrochanter for all subjects. In the largely scaling Mode 1, applied load at fracture was correlated to femoral size. Mode 2 resulted in decreased loads with an increase in medullary cavity volume and thickening of the bone. Mode 3

showed an increase in load at the onset of fracture with an increase in average bone modulus and maximum cortical bone modulus. Mode 4 showed very little change in load at onset of fracture because it was a combination of competing mechanisms. Mode 5 showed a decrease in fracture load onset with decreasing anatomical features such as femoral head diameter, femur shaft width, and intertrochanteric width (Figure 4.4). Fracture loads were in the range of experimental values (Keyak, 2000). The location of fracture initiation and patterns were sensitive to the neck-shaft angle. Fracture patterns are shown in Figure 4.5. Best and worst case subjects had fracture loads ranging from 346 N to 2827 N.

4.3.2 Effects of Intersubject Variability in Hip Fracture Repair

With a more restricted enriched region focusing around the trochanter, the mean, PCA1, and PCA2 subjects experienced an intertrochanteric fracture, which is consistent with observed clinical cases. These intertrochanteric fractures were repaired using an intramedullary implant and load transfer between the bone and implant was evaluated across the fracture plane. The repaired construct for each subject is shown in Figure 4.6. Repair models show large variations in the location and orientation of the fracture plane. Averaged normal and shear reaction forces were determined at the fracture interface for each subject (Table 4.1). In all the principal modes, the implant carried a majority of the load. In the largely scaling mode 1, there was very little change in load transfer. In mode 2, there was a significant difference in load share. PCA2_plus2 (thicker bone with a

larger medullary cavity) had a more balanced load sharing between the bone and implant than PCA2_minus2. Peak implant stresses and peak bone strains were also evaluated for each subject and are shown in Table 4.1.

4.3.3 Effects of Surgical Alignment Variability

For each implant perturbation, load share between the bone and implant, peak implant stresses and peak bone strains were evaluated. Average normal and shear reaction forces were calculated in the bone and implant across the fracture plane (Table 4.2). The perturbations bounded the range of surgical alignment variability. There were very small differences in percent load share between the bone and implant for each perturbation. However, peak implant stresses and bone strains increased for a 5 mm superior shift, and a plus and minus 5 degree internal-external rotation of the implant construct. Overall, variations in surgical alignment did not significantly alter the load transfer in the fracture repaired femur.

4.3.4 Effects of Implant Variability

Load transfer across the fracture plane was evaluated for different implant material models. A titanium alloy implant was compared to PEEK. PEEK (3.6 GPa) had a significantly smaller Young's modulus than Ti-6Al-4V (113.8 GPa), which led to a large change in load sharing between the bone and implant. In comparison to the titanium alloy, the PEEK fracture repair model had an approximately 32% shift in load

from the implant to the bone (Table 4.3). The implant carried a majority of the load in the metal implant model (73.5% implant, 26.5% bone). In PEEK, the bone carried a majority of the load (41.4% implant, 58.6% bone). The shift in load share is to be expected with a softer material. Peak implant stress was 145.4 MPa for PEEK and 217.5 MPa for Ti-6Al-4V. The PEEK implant is at-risk of failure because it is nearing the material's compressive strength (100-150 MPa). Peak bone strains were 0.003 and 0.008 for the metal and polymer implants respectively. The PEEK implant model is at-risk of implant failure and bone fracture. The results indicate that the PEEK implant would need a redesigned geometry to maintain structural integrity.

4.3.5 Effects of Loading Condition Variability

Two published loading conditions were investigated to evaluate the effects of loading on fracture repair. Percent load carried by the bone increased from the (Keyak, 2000) loading condition (73.5% implant, 26.5% bone) to the (Heller et al., 2005) loading condition (64.0% implant, 36.0% bone) (Table 4.4). In Heller et al., there were added muscle and reaction forces to represent peak forces during gait, whereas, Keyak et al. had an in-vitro, stance loading configuration with a reaction at the femoral head only. The introduction of muscle forces resulted in a more balanced load share between the bone and implant across the fracture plane. Peak implant stresses and bone strains remained relatively consistent with only a slight increase in the Heller loading condition.

4.4 Discussion

Fracture load and fracture pattern was assessed for a series of statistical model-generated subjects with varying geometry and bone quality. Predicted fracture loads were within the range of experimental in-vitro loads (Keyak, 2000). Crack patterns were representative of observed clinical cases. Fractures occurred in the neck and intertrochanteric regions. XFEM complements traditional bone analyses, which use maximum and minimum principal strain to assess fracture risk, by providing subject-specific fracture patterns without a priori knowledge of crack path. XFEM required selection of an enriched region where fracture is anticipated, but the path of crack propagation is not needed.

The current study was able to link statistical shape and intensity modeling to fracture-based finite element studies. The study provided insight into patient factors influencing fracture behavior such as fracture loads and patterns. Geometric and bone quality variables associated with fracture risk were identified using XFEM. Mode 1 indicated that smaller bones fracture at lower loads. Mode 2 showed that an increase in medullary cavity volume decreases the overall bone strength, so the fracture load also decreases. Mode 3 provided insight to bone quality factors associated with fracture risk. An increase in average bone modulus and cortical bone modulus increases the fracture load at onset. Mode 4 and mode 5 were a combination of shape and material property variability, and they showed that general increases in size can increase the strength of the bone and reduce fracture risk. Mode 4 had a large increase in neck-shaft angle, which

had very little effect on the fracture load, but it affected the location of crack initiation. Geometry with a larger neck-shaft angle fractures at a more superior/proximal location of the intertrochanter. The current study can aid clinicians by identifying shape and bone quality characteristics associated with fracture risk.

Computational models of fracture repair have the ability to evaluate implant design and clinical practice by considering subject-specific anatomy, bone quality and fracture patterns. Prior computational studies have used idealized, virtual fracture planes to assess load transfer in implant-repaired constructs (Eberle et al., 2009). The current fracture repair methodology uses fracture patterns developed from XFEM, which includes the geometric and bone quality variability of each subject. Repair models evaluated peak implant stresses, peak bone strains near the fracture, and load transfer between the bone and implant across the fracture plane. Differences in load sharing are influenced by the orientation of the fracture plane and the cross-sectional area of the bone and implant across the fracture plane. Load share was consistent in mode 1 as a result of two competing factors: implant cross-sectional area was slightly higher in PCA1_plus2, but PCA1_minus2 had significantly higher bone cross-sectional area. Since the implant cross-sectional area is the driving force in load share, mode 1 showed only small differences in load transfer. In PCA2_minus2, there was a larger implant cross-sectional area across the fracture surface than in PCA2_plus2, so the implant carried a majority of the load in PCA2_minus2. PCA2_plus2 had more balanced load sharing than PCA2_minus2. Although ideal bone healing conditions are not well understood, the

computational platform provides insight into load sharing at the fracture interface (Doblaré et al., 2004).

The effect of surgical alignment, implant material and loading condition variability was assessed using an average subject from the statistical shape and intensity model. The current evaluations on fracture repair were unique because they utilized subject-specific anatomy, bone quality, and an XFEM-derived fracture plane. Surgical alignment in superior-inferior translation and internal-external rotation of the implant-construct resulted in very little change in load share between the bone and implant across the fracture surface. Although implant alignment played a minor role in load share, peak bone strains at the fracture and peak implant stresses increased in each implant perturbation from the neutral alignment. This suggests that surgical alignment plays a larger role in implant failures and malunions.

A titanium alloy versus PEEK implant showed dramatic changes in load share between the bone and implant. Load share was dominated by the titanium implant, but with a PEEK implant, load share was dominated by the bone. The PEEK implant material had more balanced load sharing than the titanium alloy. The PEEK implant, however, was at-risk of failure and bone strains at the fracture were above the yield strain criterion. Implant geometry was not altered and results indicate that the PEEK implant would require redesigning to maintain structural integrity.

An alternate loading condition was investigated to evaluate the effects of muscle forces on hip fracture repair. The muscle-model (Heller et al., 2005) resulted in more balanced load sharing between the bone and implant across the fracture interface than the

standard in-vitro load model (Keyak, 2000). The implant carried a majority of the load in both loading scenarios, but the muscle-incorporated model carried approximately 10% more load in the bone than in the in-vitro loaded setup. Comparisons in fracture repair indicate that muscles affect load share in the bone-implant construct.

To further investigate loading on hip fracture, muscle forces were added to the fall loading condition described by Keyak et al. (2000). Strain distributions were compared between the fall and muscle-incorporated loading configurations to identify variations in potential enrichment zones for XFEM. The muscle loading configuration simulated the same oblique fall backwards and to the side as the other models, but it included maximum muscle contraction forces for the gluteus maximus, gluteus medius, gluteus minimus, ilopsoas, iliacus, and pectineus muscle bundles (Figure 4.9). Muscle attachment sites and line of action were identified by a scaled OpenSim muscle model. Origin of the muscle model coordinate system was at the center of the femoral head. Attachment patches for load distribution were determined by anatomical landmarks. A reaction load (3330N) was applied to the femoral head and the model contacted a rigid surface to simulate a fall. In the muscle-loaded model, there was an overall increase in strain because the energy in the system increased and, also, strains shifted from the neck to the trochanter (Figure 4.10). Since, intertrochanteric fractures are the most common clinical fracture, the muscle-loaded model proves the importance of muscle forces in a fall loading condition. Shifts in strain indicate that fractures are more likely to occur in the intertrochanter in future muscle-incorporated XFEM analyses.

The XFEM technique has some limitations in that, it is sensitive to localized material properties and surface segmentation. Even though XFEM can provide detailed crack paths, the technique is limited with regard to convergence. Cracks are not able to propagate all the way through the bone because the stable time increment of the analysis gets too small. This can happen if the fracture direction runs parallel to an element boundary. Despite mesh quality checks and time incrementation controls, fracture paths will inevitably run parallel to the element boundary and cause the analysis to end prematurely. In order to capture the non-linear anatomic geometry of the femur, a relatively small element size was chosen for the analyses, but this mesh density is susceptible to crack convergence issues. To improve XFEM convergence, we increased the total number of increments in the analysis, increased the number of iterations in an increment, and decreased the minimum step size. As in any finite element model, there are limitations from boundary conditions. Stress and strain values are artificial near the boundary conditions, and so fracture was excluded in the portion of the bone fixed in the trochanter. The crack surfaces in the hip repair models were extrapolated from the existing XFEM-generated fracture patterns.

The combination of statistical modeling and fracture can identify shape and bone quality characteristics that are most susceptible to fracture. As a complement to strain and risk evaluations, modeling crack initiation and growth provides further insight into hip fracture, specifically the fracture path. Fracture patterns can be uniquely defined for a population of subjects to assess fracture repair including evaluations of implant stresses, peak bone strains, and load share at the fracture, implant and surrounding bone. The

current study provides a tool for clinicians to diagnose at-risk populations and provide an engineered solution for fracture repair.

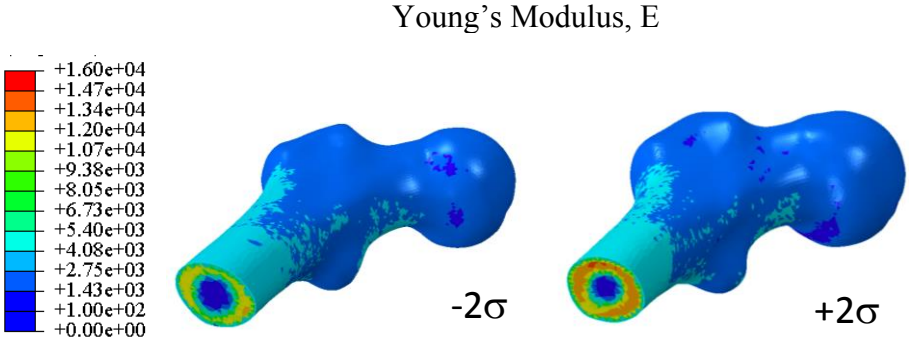

Figure 4.1: Young's modulus distribution for mode 3, which primarily captures variations in bone quality (shown at +/- 2 standard deviations)

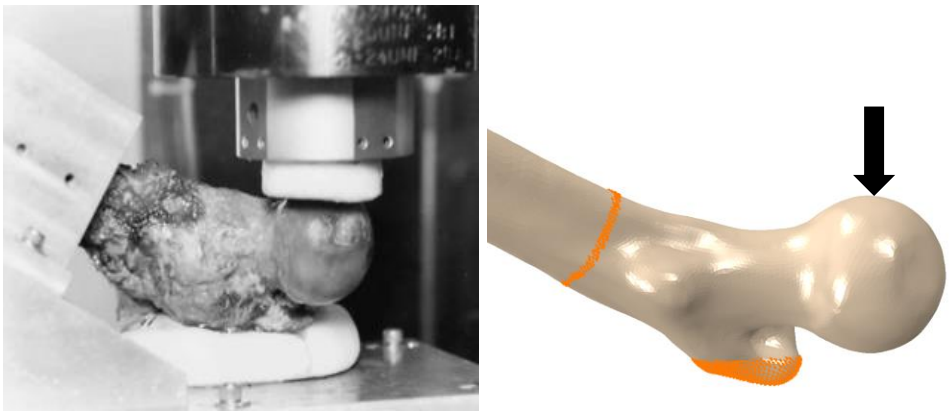

Figure 4.2: Fall loading condition with Keyak et al. 2000 (left) and model setup (right)

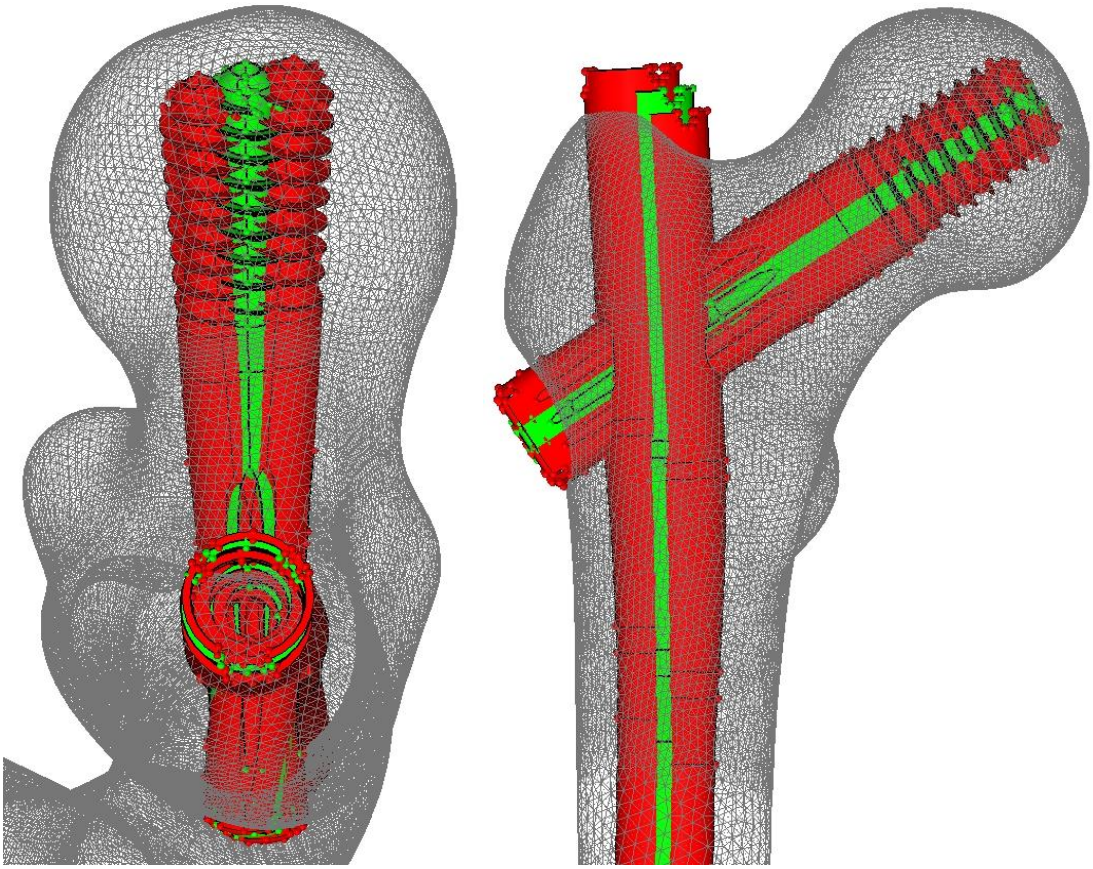

Figure 4.3: Implant perturbations for evaluating surgical alignment variability: plus and minus 5 degree internal-external rotation (left); plus and minus 5mm superior-inferior translation (right). Perturbations are shown in red and neutral alignment is shown in green.

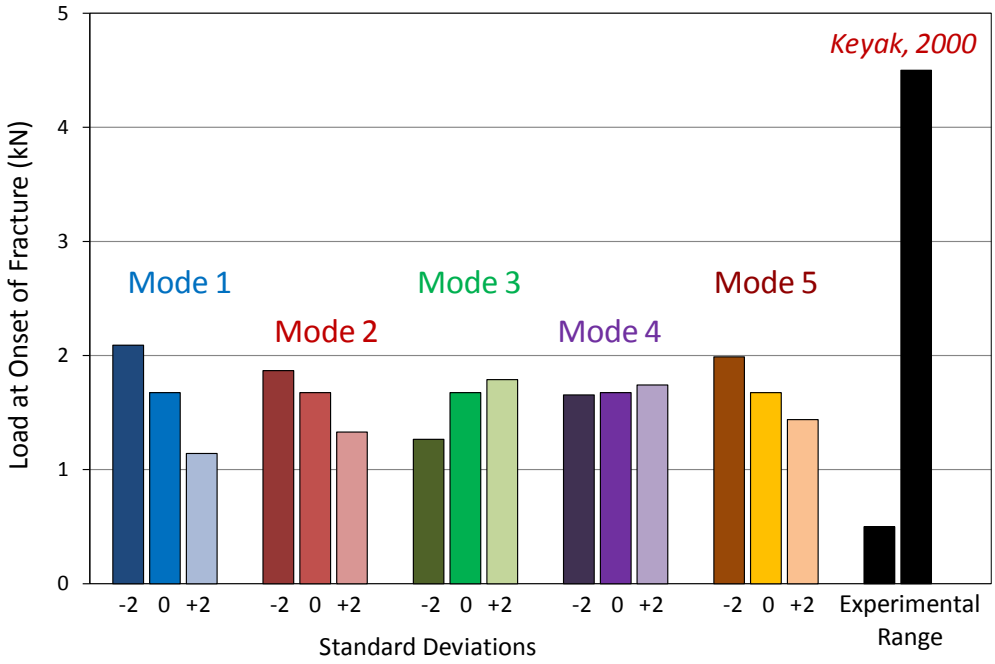

Figure 4.4: Fracture load at onset for each SSIM subject model under the fall loading condition

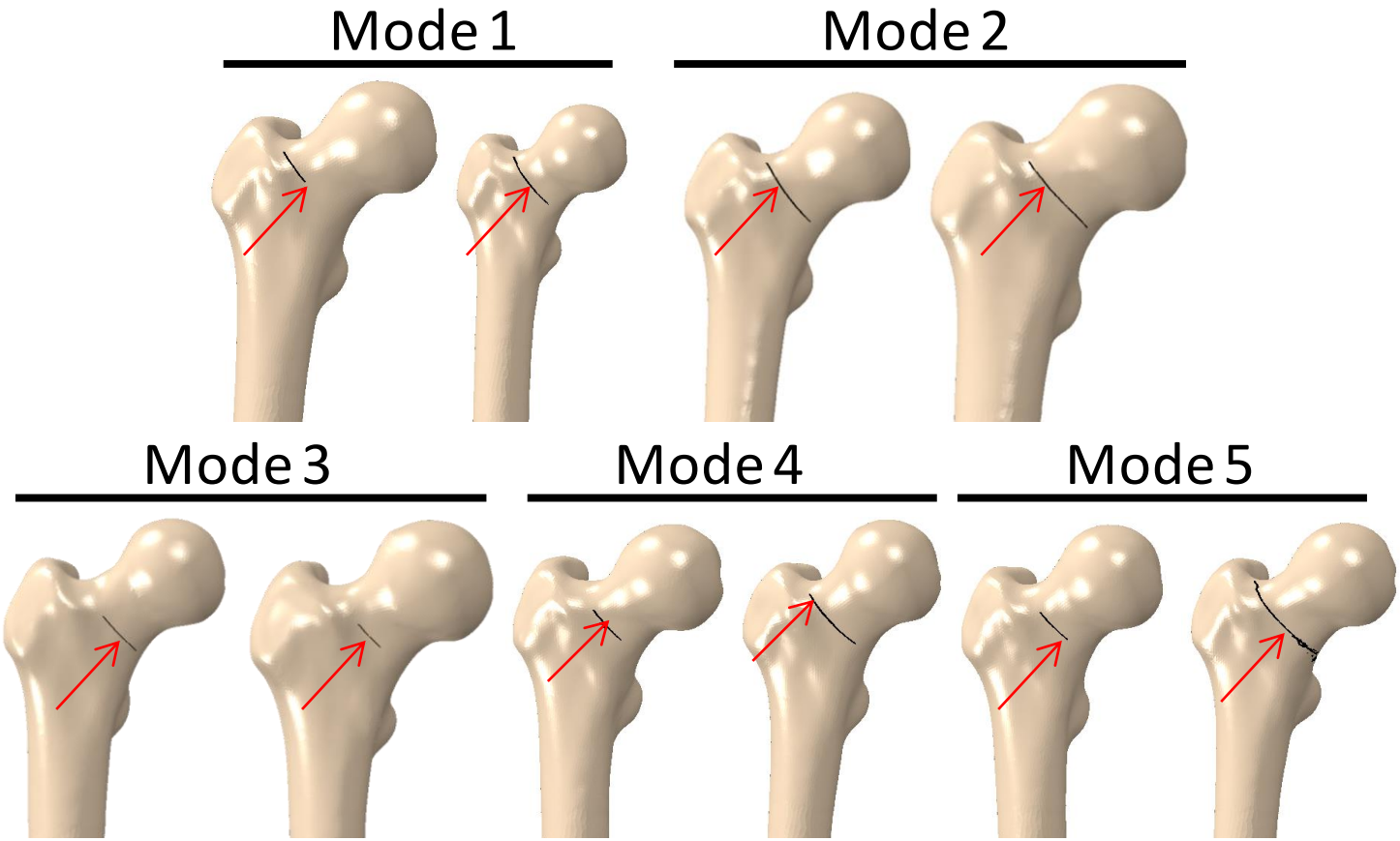

Figure 4.5: Fracture patterns for each mode of variation subjected to the fall loading condition. Crack initiation indicated by red arrows.

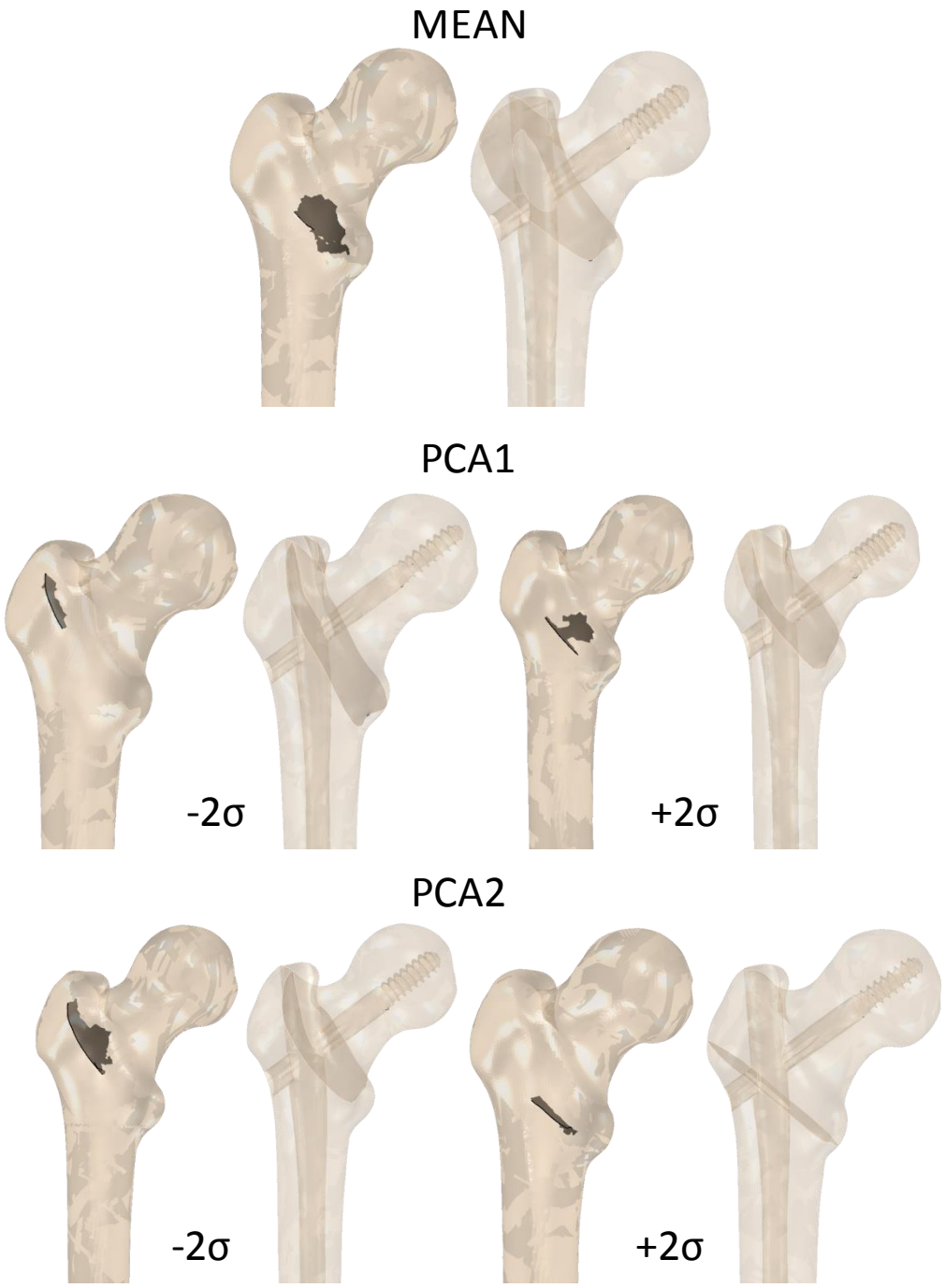

Figure 4.6: Model predicted intertrochanteric fractures and the fracture repair construct for each subject (shown at +/- 2 standard deviations)

Table 4.1: Intersubject variability results: Averaged reaction forces in the bone and implant at the fracture interface for each SSIM model including % load share, implant stress, bone strain

	Area on fracture plane (mm^2)	Normal force (N)	Shear force (N)	Total force (N)	% Load	Peak Implant Stress (MPa)	Peak Bone Strain
Mean							
Bone	1931.1	2047.8	1219.0	2383.1	26.5	217.457	0.0027
Implant	406.2	5079.6	4235.7	6613.9	73.5		
PCA1_MINUS2							
Bone	2707.9	1765.5	1133.8	2098.2	19.1	312.869	0.0052
Implant	531.9	7950.4	4003.6	8901.5	80.9		
PCA1_PLUS2							
Bone	1112.4	1788.9	1233.1	2172.7	20.0	892.4	0.0050
Implant	572.2	7333.0	4712.4	8716.6	80.0		
PCA2_MINUS2							
Bone	1108.6	1518.7	1300.3	1999.3	26.9	289.922	0.0037
Implant	355.1	4906.1	2310.9	5423.1	73.1		
PCA2_PLUS2							
Bone	2192.6	2167.6	950.3	2366.8	35.3	207.712	0.0052
Implant	287.4	3642.4	2345.2	4332.1	64.7		

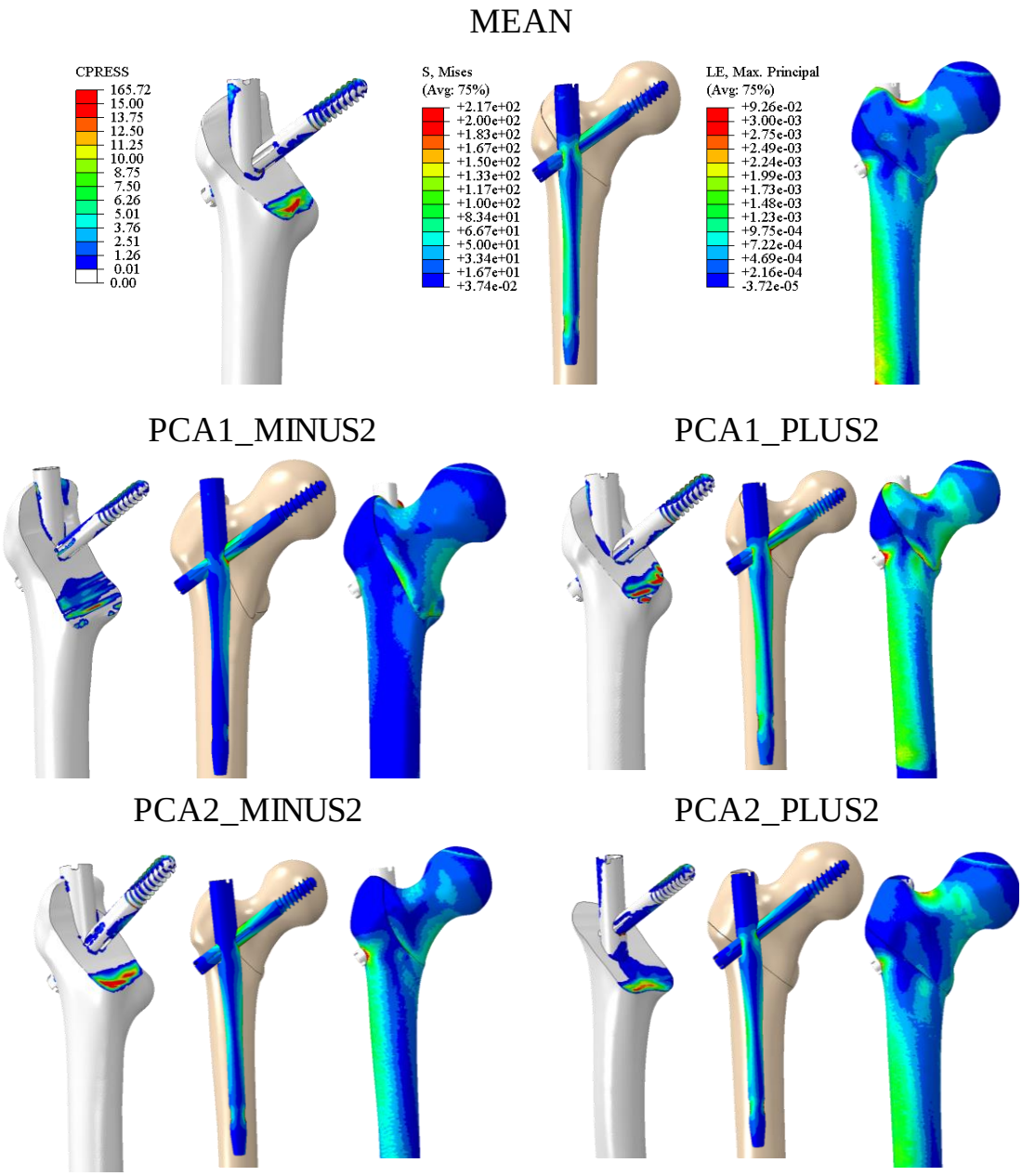

Figure 4.7: Contact pressure, implant Von Mises stress, and bone strain for each subject femur model.

Table 4.2: Results of surgical alignment variability: Averaged reaction forces in the bone and implant at the fracture interface for each implant perturbation including % load share, implant stress, bone strain

	Area on fracture plane (mm^2)	Normal force (N)	Shear force (N)	Total force (N)	% Load	Peak Implant Stress (MPa)	Peak Bone Strain
Neutral							
Bone	1931.1	2047.8	1219.0	2383.1	26.5	217.457	0.0027
Implant	406.2	5079.6	4235.7	6613.9	73.5		
S-I + 5mm							
Bone	1909.4	2153.8	1316.1	2524.1	26.4	321.770	0.0038
Implant	429.6	5449.2	4427.0	7020.8	73.6		
S-I – 5mm							
Bone	1961.0	2190.4	1264.4	2529.1	26.9	218.400	0.0026
Implant	377.7	5415.5	4233.8	6874.1	73.1		
I-E + 5deg							
Bone	1948.2	2208.8	1332.6	2579.7	27.4	335.668	0.0033
Implant	389.6	5452.3	4142.9	6847.7	72.6		
I-E – 5deg							
Bone	1905.2	2239.4	1303.3	2591.1	29.2	327.958	0.0044
Implant	433.5	4835.9	3999.4	6275.4	70.8		

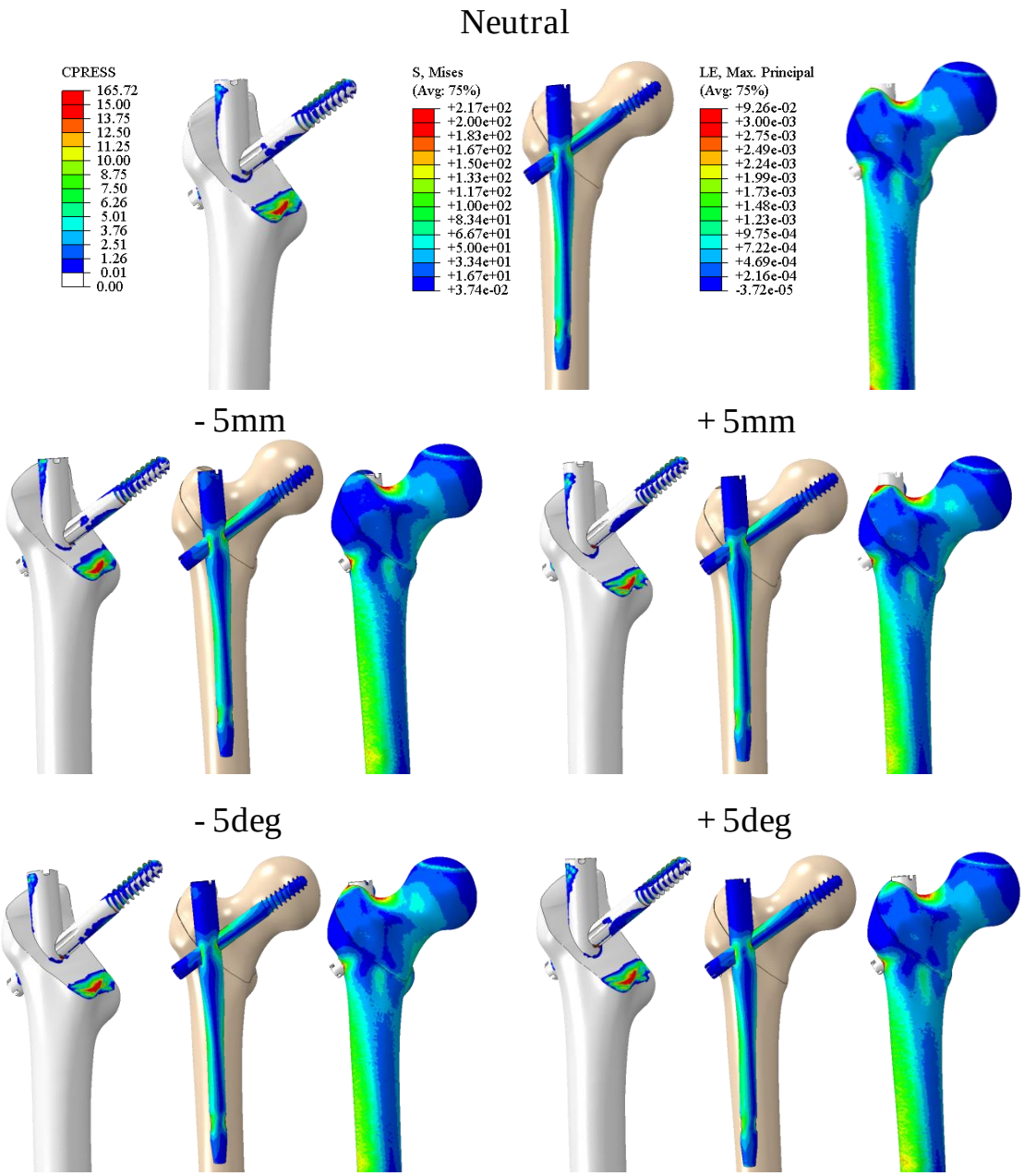

Figure 4.8: Contact pressure, implant Von Mises stress, and bone strain for each implant perturbation in surgical alignment.

Table 4.3: Results of implant variability: Averaged reaction forces in the bone and implant at the fracture interface for each implant material including % load share, implant stress, bone strain

	Area on fracture plane (mm^2)	Normal force (N)	Shear force (N)	Total force (N)	% Load	Peak Implant Stress (MPa)	Peak Bone Strain
Ti-6Al-4V							
Bone	1931.1	2047.8	1219.0	2383.1	26.5	217.457	0.0027
Implant	406.2	5079.6	4235.7	6613.9	73.5		
PEEK							
Bone	1931.1	2655.0	1893.5	3261.0	58.6	145.392	0.0083
Implant	406.2	1776.0	1470.3	2305.6	41.4		

Table 4.4: Results of loading condition variability: Averaged reaction forces in the bone and implant at the fracture interface for each load profile including % load share, implant stress, bone strain

	Area on fracture plane (mm^2)	Normal force (N)	Shear force (N)	Total force (N)	% Load	Peak Implant Stress (MPa)	Peak Bone Strain
Keyak et al. 2000							
Bone	1931.1	2047.8	1219.0	2383.1	26.5	217.457	0.0027
Implant	406.2	5079.6	4235.7	6613.9	73.5		
Heller et al. 2005							
Bone	1931.1	3037.1	1832.3	3547.0	36.0	248.427	0.0032
Implant	406.2	4720.7	4169.6	6298.5	64.0		

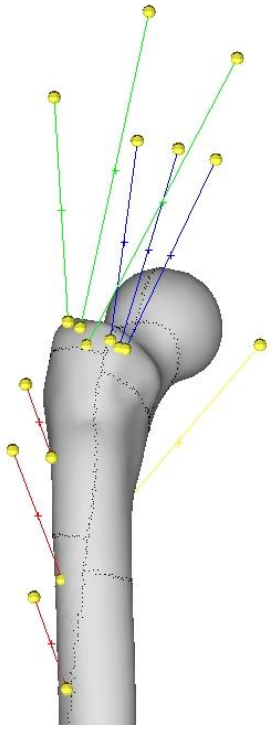

Figure 4.9: Fall loading with added muscle forces: gluteus maximus, gluteus medius, gluteus minimus, iliopsoas, iliacus, and pectineus

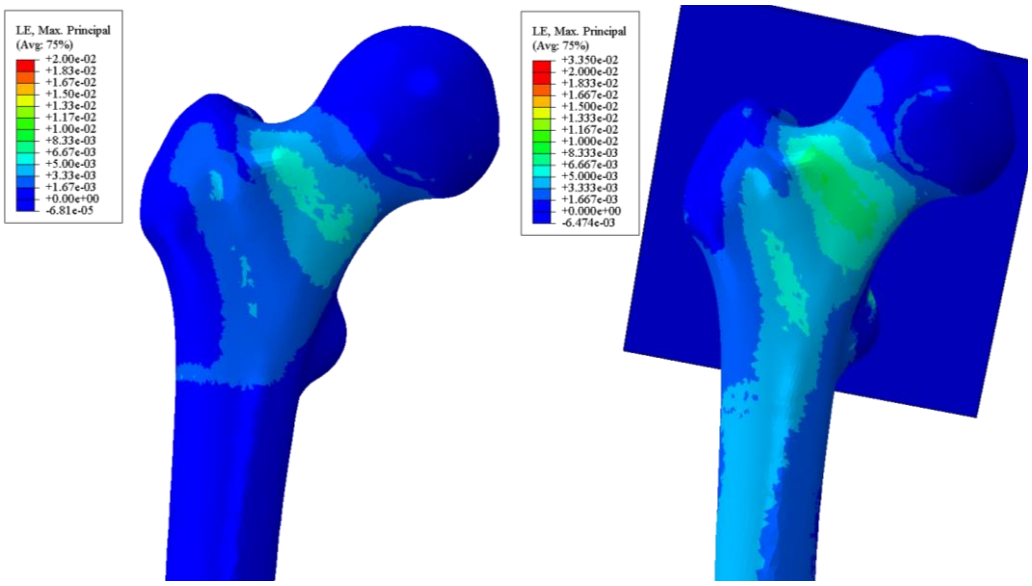

Figure 4.10: Strain distribution comparison between in-vitro fall loading condition (left) and including contributions of muscle forces (right)

Chapter 5. Conclusions and Recommendations

The studies presented in this thesis are a series of work representing the progression of computational modeling of hip fracture and repair. The study developed a novel computational approach to predict fracture patterns in a population of subjects, and a platform for evaluating fracture repair considering surgical alignment, implant, and loading condition variability. The extended finite element method (XFEM) was used to simulate the location of crack initiation and the path of crack-propagation in subject-specific femur models with varying patient anatomy and bone quality. Specific emphasis was placed on verifying model predictions of fracture patterns to experimental in-vitro testing in order to ensure the accuracy of the technique. The development of FE models can be challenging due to the substantial time and specific knowledge required to construct complex anatomic geometries and perform model pre-processing and post-processing. However, a developed FE model can be used to evaluate varying loading and boundary conditions, and perform probabilistic analyses. The hip fracture model was able to predict accurate fracture patterns considering patient variability. Alternate loading conditions could be investigated to identify a more physiological representation of a fall and trochanteric fractures. Although crack patterns were predicted well, the XFEM technique was not able to predict fracture loads well due to the sensitivity in material properties and local segmentation. In order to make the technique well-rounded,

material property assignment would need improved resolution to properly capture thin cortical layers of bone in the proximal section of the femur.

In application to implant design and fracture repair, the study developed a methodology to quantify load share across subject-specific fracture planes. The effects of patient, surgical, implant and loading variability on hip fracture repair were assessed. The suite of computational tools presented in this study could be used to evaluate implant design and identify ideal bone healing conditions. Validation of the fracture repair technique is difficult due to the complexity and accuracy of the experimental setup. However, a comparison between model and experiment of a fracture repaired specimen would add validity and confidence to the model findings. In this study, individual perturbations of surgical alignment were performed to assess the effects of implant alignment on hip fracture repair. Probabilistic analysis allows for simultaneous considerations of alignment variability in contrast to using individual perturbations. In order to perform probabilistic analyses, an automated model generation technique would need to be developed to place the implant, mesh the surrounding bone, map bone properties, and run the finite element analysis. Latin Hypercube could be used to capture the design space of the SSIM model and create a wide range of fracture patterns representative of the population. Monte Carlo simulations and Advanced Mean Value techniques could be applied to the SSIM model to capture the variability in surgical alignment on fracture repair.

List of References

Areias, P.M., Belytschko, T., 2005. Analysis of three-dimensional crack initiation and propagation using the extended finite element method. International Journal for Numerical Methods in Engineering 63, 760–788.

ASTM Standard E8, 2012, "Standard Test Methods for Tension Testing of Metallic Materials" ASTM International, West Conshohocken, PA, 2012, DOI: 10.1520/E0008_E0008M-11, www.astm.org.

Bauer, D.C., Ewing, S.K., Cauley, J. a, Ensrud, K.E., Cummings, S.R., Orwoll, E.S., 2007. Quantitative ultrasound predicts hip and non-spine fracture in men: the MrOS study. Osteoporosis international : a journal established as result of cooperation between the European Foundation for Osteoporosis and the National Osteoporosis Foundation of the USA 18, 771–7.

Bauer, D.C., Garnero, P., Harrison, S.L., Cauley, J.A., Eastell, R., Ensrud, K.E., 2009. Biochemical Markers of Bone Turnover, Hip Bone Loss, and Fracture in Older Men: The MrOS Study. Journal of Bone and Mineral Research 24, 2032–2038.

Belytschko, T., Black, T., 1999. Elastic crack growth in finite elements. International Journal for Numerical Methods in Engineering 620, 601–620.

Brauer, C. a, Coca-Perraillon, M., Cutler, D.M., Rosen, A.B., 2009. Incidence and mortality of hip fractures in the United States. Journal of American Medical Association 302, 1573–9.

Brauer, C.A., Coca-Peraillon, M., Cutler, D.M., Rosen, A.B., 2009. Incidence and Mortality of Hip Fractures in the United States. Journal of American Medical Association 302, 1573–1579.

Bryan, R., Mohan, P.S., Hopkins, A., Galloway, F., Taylor, M., Nair, P.B., 2010. Statistical modelling of the whole human femur incorporating geometric and material properties. Medical Engineering & Physics 32, 57–65.

Bryan, R., Nair, P.B., Taylor, M., 2009. Use of a statistical model of the whole femur in a large scale, multi-model study of femoral neck fracture risk. Journal of Biomechanics 42, 2171–6Cook, R.B., Zioupos, P., 2009. The fracture toughness of cancellous bone. Journal of Biomechanics 42, 2054–60.

Cristofolini, L., Schileo, E., Juszczyk, M., Taddei, F., Martelli, S., Viceconti, M., 2010. Mechanical testing of bones: the positive synergy of finite-element models and in vitro experiments. Philosophical transactions. Series A, Mathematical, physical, and engineering sciences 368, 2725–63.

Cristofolini, L., Juszczyk, M., Martelli, S., Taddei, F., Viceconti, M., 2007. In vitro replication of spontaneous fractures of the proximal human femur. Journal of Biomechanics 40, 2837–2845.

Cummings, S.R., Melton, L.J., 2002. Epidemiology and outcomes of osteoporotic fractures. Lancet 359, 1761–7.

Doblaré, M., García, J.M., Gómez, M.J., 2004. Modelling bone tissue fracture and healing: a review. Engineering Fracture Mechanics 71, 1809–1840.

Dall'Ara, E., Luisier, B., Schmidt, R., Kainberger, F., Zysset, P., Pahr, D., 2013. A nonlinear QCT-based finite element model validation study for the human femur tested in two configurations in vitro. Bone 52: 27-38.

Eberle, S., Bauer, C., Gerber, C., Von Oldenburg, G., Augat, P., 2010. The stability of a hip fracture determines the fatigue of an intramedullary nail. Proceedings of the Institution of Mechanical Engineers, Part H: Journal of Engineering in Medicine 224, 577–584.

Eberle, S., Gerber, C., Von Oldenburg, G., Hungerer, S., Augat, P., 2009. Type of hip fracture determines load share in intramedullary osteosynthesis. Clinical Orthopaedics and Related Research 467, 1972–80.

Eberle, S., Gerber, C., Von Oldenburg, G., Högel, F., Augat, P., 2010. A biomechanical evaluation of orthopaedic implants for hip fractures by finite element analysis and *in-vitro* tests. Proceedings of the Institution of Mechanical Engineers, Part H: Journal of Engineering in Medicine 224, 1141–1152.

Eberle, S., Göttlinger, M., Augat, P., 2012. An investigation to determine if a single validated density-elasticity relationship can be used for subject specific finite element analyses of human long bones. Medical Engineering & Physics.

Eberle, S., Göttlinger, M., Augat, P., 2013. Individual density–elasticity relationships improve accuracy of subject-specific finite element models of human femurs. Journal of Biomechanics 46, 2152–2157

Elkins, J.M., Pedersen, D.R., Callaghan, J.J., Brown, T.D., 2013. Do Obesity and/or Stripe Wear Increase Ceramic Liner Fracture Risk? An XFEM Analysis. Clinical orthopaedics and related research 471, 527–36.

Fitzpatrick, C.K., Baldwin, M.A., Ali, A.A., Laz, P.J., Rullkoetter, P.J., 2011. Comparison of patellar bone strain in the natural and implanted knee during simulated deep flexion. Journal of Orthopaedic Research 29, 232-239.

Fritscher, K., Grunerbl, A., Hanni, M., Suhm, N., Hengg, C., Schubert, R., 2009. Trabecular bone analysis in CT and X-ray images of the proximal femur for the assessment of local bone quality. IEEE Transactions on Medical Imaging 28, 1560–75.

Gracie, R., Oswald, J., Belytschko, T., 2008. On a new extended finite element method for dislocations: Core enrichment and nonlinear formulation. Journal of the Mechanics and Physics of Solids 56, 200–214.

Hall, M.J., DeFrances, C.J., Williams, S.N., Golosinskiy, A., Schwartzman, A., 2010. National Hospital Discharge Survey: 2007 Summary. National Health Statistics Reports 1–20, 24.

Hambli, R., Bettamer, A., Allaoui, S., 2012. Finite element prediction of proximal femur fracture pattern based on orthotropic behaviour law coupled to quasi-brittle damage. Medical Engineering and Physics 34, 202–210.

Hambli R., Benhamou, C.-L., Jennane, R., Lespessailles, E., Skalli, W., Laporte, S., Laredo, J.-D., Bousson, V., Zarka, J., 2013A. Combined finite element model of human proximal femur behavior considering remodeling and fracture. IRBM, 191-195.

Hambli, R., 2013B. A quasi-brittle continuum damage finite element model of the human proximal feur based on element deletion. Medical & Biological Engineering & Computing 51:219-231.

Helgason B, Perilli E, Schileo E, Taddei F, Brynjólfsson S, Viceconti M., 2008. Mathematical relationships between bone density and mechanical properties: a literature review. Clinical Biomechanics (Bristol, Avon) 23, 135–46.

Heller, M.O., Bergmann, G., Kassi, J.-P., Claes, L., Haas, N.P., Duda, G.N., 2005. Determination of muscle loading at the hip joint for use in pre-clinical testing. Journal of Biomechanics 38, 1155–63.

Hughes, T.J.R., Belytschko, T., 2010. A generalized finite element formulation for arbitrary basis functions : From isogeometric analysis to XFEM. International Journal for Numerical Methods in Engineering 83, 765–785.

Huynh, D.B.P., Belytschko, T., 2009. The extended finite element method for fracture in composite materials. International Journal for Numerical Methods in Engineering 77, 214–239.

Johnell, O., Kanis, J., 2006. An estimate of the worldwide prevalence and disability associated with osteoporotic fractures. Osteoporosis International 17, 1726–33.

Juszczyk, M.M., Cristofolini, L., Viceconti, M., 2011. The human proximal femur behaves linearly elastic up to failure. Journal of Biomechanics 44, 2259–2266.

Kalender, W.A., 1992. A phantom for standardization and quality control in spinal bone mineral measurements by QCT and DXA: Design considerations and specifications. Medical Physics 19, 583-586.

Kaptoge, S., Beck, T.J., Reeve, J., Stone, K.L., Hillier, T.A., Cauley, J.A., Cummings, S.R., 2008. Prediction of Incident Hip Fracture Risk by Femur Geometry Variables Measured by Hip Structural Analysis in the Study of Osteoporotic Fractures. Journal of Bone and Mineral Research 23, 1892–1904.

Kaufer, H., 1980. Mechanics of the treatment of hip injuries. Clinical Orthopaedics and Related Research, *146*, 53-61.

Keyak, J.H., 2000. Relationships between femoral fracture loads for two load configurations. Journal of Biomechanics 33, 499–502.

Keyak, J.H., Falkinstein, Y., 2003. Comparison of in situ and in vitro CT scan-based finite element model predictions of proximal femoral fracture load. Medical Engineering and Physics 25, 781–787.

Krug, R., Banerjee, S., Han, E.T., Newitt, D.C., Link, T.M., Majumdar, S., 2005. Feasibility of in vivo structural analysis of high-resolution magnetic resonance images of the proximal femur. Osteoporosis International 16, 1307–14.

Laz, P.J., Stowe, J.Q., Baldwin, M. A., Petrella, A.J., Rullkoetter, P.J., 2007. Incorporating uncertainty in mechanical properties for finite element-based evaluation of bone mechanics. Journal of Biomechanics 40, 2831–6.

Les, C.M., Keyak, J.H., Stover, S.M., Taylor, K.T., Kaneps, a J., 1994. Estimation of material properties in the equine metacarpus with use of quantitative computed tomography. Journal of Orthopaedic Research 12, 822–33.

Liu, X., Qin, X., Du, Z., 2010. Bone Fracture Analysis Using the Extended Finite Element Method (XFEM) with Abaqus. American Society of Biomechanics.

Morgan, E.F., Bayraktar, H.H., Keaveny, T.M., 2003. Trabecular bone modulus–density relationships depend on anatomic site. Journal of Biomechanics 36, 897–904.

Morgan, E.F., Keaveny, T.M., 2001. Dependence of yield strain of human trabecular bone on anatomic site. Journal of Biomechanics 34, 569–77.

Orwoll, E., Blank, J.B., Barrett-Connor, E., Cauley, J., Cummings, S., Ensrud, K., Lewis, C., Cawthon, P.M., Marcus, R., Marshall, L.M., McGowan, J., Phipps, K., Sherman, S., Stefanick, M.L., Stone, K., 2005. Design and baseline characteristics of the osteoporotic fractures in men (MrOS) study--a large observational study of the determinants of fracture in older men. Contemporary Clinical Trials 26, 569–85.

Peng, L., Bai, J., Zeng, X., Zhou, Y., 2006. Comparison of isotropic and orthotropic material property assignments on femoral finite element models under two loading conditions. Medical Engineering & Physics 28, 227–33.

Raunest, J., Englemann, R., Jonas, M., Derra, E., 2001. Morbidity and mortality in para-articular femoral fractures in advanced age. Unfallchirug 104, 325–332.

Rho, J.Y., Scottish, T., Hospital, R., 1995. Relations of mechanical properties CT numbers in human bone. Medical Engineering & Physics 17, 347–355.

Schileo, E., Dall'ara, E., Taddei, F., Malandrino, A., Schotkamp, T., Baleani, M., Viceconti, M., 2008. An accurate estimation of bone density improves the accuracy of subject-specific finite element models. Journal of Biomechanics 41, 2483–91.

Schileo, E., Taddei, F., Cristofolini, L., Viceconti, M., 2008. Subject-specific finite element models implementing a maximum principal strain criterion are able to estimate failure risk and fracture location on human femurs tested in vitro. Journal of Biomechanics 41, 356–67.

Song, J.-H., Wang, H., Belytschko, T., 2007. A comparative study on finite element methods for dynamic fracture. Computational Mechanics 42, 239–250.

Taddei, F., Cristofolini, L., Martelli, S., Gill, H.S., Viceconti, M., 2006. Subject-specific finite element models of long bones: An in vitro evaluation of the overall accuracy. Journal of Biomechanics 39, 2457–67.

Taddei, F., Martelli, S., Reggiani, B., Cristofolini, L., Viceconti, M., 2006. Finite-element modeling of bones from CT data: sensitivity to geometry and material uncertainties. IEEE Transactions on bio-medical engineering 53, 2194–200.

Taylor, M., 2006. Finite Element Analysis of the resurfaced femoral head. Journal of Engineering in Medicine 68, 289-297.

Trabelsi, N., Yosibash, Z., Wutte, C., Augat, P., Eberle, S., 2011. Patient-specific finite element analysis of the human femur - A double-blinded biomechanical validation Journal of Biomechanics 44, 1666–1672.

Ural, A., Bruno, P., Zhou, B., Shi, X.T., Guo, X.E., 2013A. A new fracture assessment approach coupling HR-pQCT imaging and fracture mechanics-based finite element modeling. Journal of Biomechanics 46, 1305–1311.\

Ural, A., Mischinski, S., 2013B. Multiscale modeling of bone fracture using cohesive finite elements. Engineering Fracture Mechanics 103, 141–152.

Wille, H., Rank, E., Yosibash, Z., 2012. Prediction of the mechanical response of the femur with uncertain elastic properties. Journal of Biomechanics 45, 1140–8.

Zimmermann, E., Launey, M.E., Barth, H.D., Ritchie, R.O., 2009. Mixed-mode fracture of human cortical bone. Biomaterials 30, 5877–84.